

และที่นิยมกันมาก ก็คือ การใช้สารเฟอร์โรอิเล็กทริกชนิดอื่นๆ ที่เตรียมได้ง่ายกว่า เช่น PZT หรือ PT หรือ BT เข้ามาช่วยในการสร้างเสถียรภาพของเฟสเพอโรฟสไกต์ให้แก่ระบบเพื่อจะได้นำศักยภาพของสาร PZN ไปใช้ประโยชน์ได้ เป็นต้น [16,25,26]

สำหรับงานวิจัยที่เกี่ยวข้องโดยตรงกับเรื่องสาร $ZnNb_2O_6$ นั้นก็เริ่มมีปรากฏออกมาบ้างแล้ว แต่ส่วนมากจะเน้นไปที่เรื่องของการศึกษาสมบัติไมโครเวฟไดอิเล็กทริกของสารชนิดนี้เป็นหลัก [27-29] ทางผู้วิจัยจึงมีความสนใจที่จะทำการศึกษาและพัฒนากระบวนการสังเคราะห์สาร $ZnNb_2O_6$ ด้วยเทคนิค solid-state reaction ซึ่งก็จะรวมไปถึงการศึกษาวิจัยในเรื่องของการประดิษฐ์เซรามิก PZN โดยใช้ $ZnNb_2O_6$ เป็นสารตั้งต้นด้วย นอกจากนี้การปรับปรุงและพัฒนาสมบัติทางไฟฟ้าของสารเซรามิก เฟอร์โรอิเล็กทริกเพื่อนำไปประยุกต์ใช้ทางด้านอิเล็กทรอนิกส์ ส่วนใหญ่มักนิยมเติมสารออกไซด์ ชนิดต่างๆ [30-35] เช่น Nb_2O_5 , Fe_2O_3 , MnO_2 รวมไปถึงสารเฟอร์โรอิเล็กทริกชนิดอื่นๆ ที่เตรียมได้ ง่ายกว่า เช่น BT [36] หรือ PT [37] หรือ PZT [38] เข้าไปเพื่อช่วยพัฒนาสมบัติทางไฟฟ้า อีกทั้ง ยังมีรายงานว่าวิธีดังกล่าวสามารถทำให้เฟสเพอโรฟสไกต์มีความเสถียรภาพ [18,36-39] ซึ่งผู้วิจัยเอง ก็มีประสบการณ์ในการทำงานวิจัยที่เกี่ยวข้องกับการพัฒนาสารในระบบ PZN-PZT มาบ้างแล้ว [40-41] ทางผู้วิจัยมีความสนใจที่ทำการศึกษาพฤติกรรมการเกิดของเฟสเพอโรฟสไกต์ โครงสร้างจุลภาคและสมบัติทางไฟฟ้าของสาร PZN ที่มีการเติมสารออกไซด์ชนิดต่างๆ เช่น MnO_2 , Fe_2O_3 และ Al_2O_3 ลงไปด้วย โดยคาดว่าจะได้ข้อมูลใหม่ๆ ที่สามารถนำไปใช้ในการพัฒนาแนวทางการวิจัยเพื่อเสริมกับองค์ความรู้พื้นฐานเดิมที่มีอยู่และมีผลสืบเนื่องต่อการนำไปตีพิมพ์เผยแพร่ใช้งานต่อไป เนื่องจากยังไม่มีรายงานผลการศึกษาในประเด็นนี้มาก่อน

เอกสารอ้างอิง

- [1] A.J. Moulson and J.M. Herbert, *Electroceramics*, 2nd ed., Wiley-Interscience, Chichester, 2003.
- [2] R.C. Buchanan, *Ceramic Materials for Electronics*, 3rd ed., Marcel Dekker, New York, 2004.
- [3] A.S. Bhalla, R. Guo and R. Roy, *Mater. Res. Innov.* **4**, 3 (2000).
- [4] L.E. Cross, *Ferroelectrics*. **151**, 305 (1994).
- [5] N. Setter and R. Waser, *Acta Mater.* **48**, 151 (2000).
- [6] S.E. Park and T.R. Shrout, *Mater. Res. Innov.* **1**, 20 (1997).
- [7] สุพล อนันตา, การพัฒนากระบวนการเตรียมสาร PZT โดยวิธีการประยุกต์กระบวนการผสมออกไซด์แบบ 2 ขั้นตอน, รายงานฉบับสมบูรณ์โครงการทุนวิจัยหลังปริญญาเอก, สนับสนุนโดยสำนักงานกองทุนสนับสนุนการวิจัย (สกว.) พ.ศ. 2545.
- [8] W. Chaisan, S. Ananta and T. Tunkasiri, *Curr. Appl. Phys.* **4**, 182 (2004).
- [9] A. Udomporn and S. Ananta, *Mater. Lett.* **58**, 1154 (2004).

- [10] W. Chaisan, R. Yimnirun, S. Ananta and D.P. Cann, *Mater. Lett.* **59**, 3732 (2005).
- [11] R. Wongmaneerung, R. Yimnirun and S. Ananta, *Mater. Lett.* **60**, 1452 (2006).
- [12] K. Uchino, *Ferroelectric Devices*, Marcel Dekker, New York, 2000.
- [13] G.H. Haertling, *J. Am. Ceram. Soc.* **82**, 797 (1999).
- [14] K. Uchino, *Solid State Ionics.* **108**, 43 (1998).
- [15] J. wang, J. Xue and D. Wan, *Solid State Ionics.* **127**, 169 (2000).
- [16] A. Halliyal, U. Kumar, R.E. Newnham and L.E. Cross, *Am. Ceram. Soc. Bull.* **66**, 671 (1987).
- [17] M.M.A. Sekar and A. Halliyal, *J. Am. Ceram. Soc.* **81**, 380 (1998).
- [18] T.R. Shrout and A. Halliyal, *Am. Ceram. Soc. Bull.* **66**, 704 (1987).
- [19] N. Wakiya, N. Ishizawa, K. Shinazaki and N. Mizutani, *Mater. Res. Bull.* **30**, 1121 (1995).
- [20] M. Villegas, A.C. Caballerc, C. Moure, P. Duran, J.F. Fernandez and R.E. Newnham, *J. Am. Ceram. Soc.* **83**, 141 (2000).
- [21] C.L. Li and C.C. Chou, *Integr. Ferroelectr.* **55**, 955 (2003).
- [22] Y. Matsuo, H. Sasaki, S. Hayakawa, F. Kanamura and M. Koizumi, *J. Am. Ceram. Soc.* **52**, 516 (1969).
- [23] J.M. Hayes, T.R. Gururaja, G.L. Geoffroy and L.E. Cross, *J. Mater. Sci. Lett.* **5**, 396 (1987).
- [24] R. Palai, S. Sharma and R.N.P. Choudhary, *J. Mater. Sci. Lett.* **20**, 1237 (2001).
- [25] N. Vittayakorn, G. Rujijanagul, T. Tunkasiri, X. Tan and D.P. Cann, *Mat. Sci. Eng. B* **108**, 258 (2004).
- [26] W. Zhu, A.L. Kholkin, P.Q. Mantas and J.L. Baptista, *J. Am. Ceram. Soc.* **84**, 1740 (2001).
- [27] L.B. Kong, J. Ma, H. Huang, R.F. Zhang and T.S. Zhang, *J. Alloy. Compd.* **347**, 308 (2002).
- [28] Y.C. Zhang, Z.X. Yue, Z.L. Gui and L.T. Li, *Ceram. Int.* **29**, 555 (2003).
- [29] R.C. Pullar, J.D. Breeze and N. McN. Alford, *J. Am. Ceram. Soc.* **88**, 2466 (2005).
- [30] T. Kala, *Phase Transitions*, **36**, 65 (1991).
- [31] T.K. Vasileva, M.M. Nadoliisky and S.D. Toshev, *Phys. Status Solidi. (a).*, **86**, 109 (1984).
- [32] S. Takahashi and M. Takahashi, *Jpn. J. Appl. Phys.*, **11**, 31 (1972)
- [33] K. Toshio, S. Toshimasa and T. Takaaki, *Jpn. J. Appl. Phys.*, **31**, 3058 (1992)
- [34] J. S. Kim, K. H. Yoon, B. H. Choi, J. O. Park, and J. M. Lee, *J. Kor. Ceram. Soc.*, **27**, 187 (1990).
- [35] H. Yudong, Z. Mankang and G. Feng, *J. Am. Ceram. Soc.*, **87**, 847 (2004).
- [36] A. Halliyal, U. Kumar, and R. E Newnham, *Am. Ceram. Soc. Bull.* **66**, 671 (1987).
- [37] J. R. Belsick, A. Halliyal, U. Kumar, and R. E. Newnham, *Am. Ceram. Soc. Bull.* **66**, 664 (1987).
- [38] H.Q. Fan and H.E. Kim, *J. Am. Ceram. Soc.*, **84**, 636 (2001).
- [39] N. Vittayakorn, G. Rujijanagul, T. Tunkasiri, X. Tan, D.P. Cann, *J. Mater. Sci. and Eng. B.*, **108**, 258 (2004).



สำนักงานคณะกรรมการวิจัยแห่งชาติ	
ห้องสมุดงานวิจัย	
วันที่.....	9 10 2555
เลขทะเบียน.....	247627
เลขเรียกหนังสือ.....	

2. วัตถุประสงค์

- 2.1 เพื่อศึกษาอิทธิพลของปัจจัยในกระบวนการสังเคราะห์สารเพอร์โรอิเลกทริก $Pb(Zn_{1/3}Nb_{2/3})O_3$ ด้วยเทคนิค mixed oxide แบบดัดแปลงที่ใช้ $ZnNb_2O_6$ เป็นสารตั้งต้นที่มีต่อพฤติกรรมการก่อเกิดเฟส สัณฐานวิทยาและองค์ประกอบทางเคมีระดับจุลภาคเปรียบเทียบกับวิธีการเตรียมแบบดั้งเดิม
- 2.2 เพื่อศึกษาอิทธิพลของการเผาซินเทอร์ที่มีต่อพฤติกรรมการก่อเกิดเฟส โครงสร้างจุลภาคและสมบัติทางไฟฟ้าของเซรามิก $Pb(Zn_{1/3}Nb_{2/3})O_3$
- 2.3 เพื่อศึกษาอิทธิพลของการเติมสารออกไซด์ชนิดต่างๆที่มีต่อพฤติกรรมการก่อเกิดเฟส โครงสร้างจุลภาคและสมบัติทางไฟฟ้าของเซรามิก $Pb(Zn_{1/3}Nb_{2/3})O_3$
- 2.4 เพื่อตีพิมพ์เผยแพร่ผลการวิจัยลงในวารสารวิชาการระดับนานาชาติ รวมทั้งการนำเสนอในที่ประชุมวิชาการทั้งในและต่างประเทศ

3. วิธีทดลอง

โครงการวิจัยนี้ประกอบด้วยระเบียบวิธีวิจัย 2 ส่วนหลัก คือ

- [1] การประดิษฐ์และตรวจสอบเซรามิก $Pb(Zn_{1/3}Nb_{2/3})O_3$ ที่เตรียมด้วยวิธี mixed oxide แบบดัดแปลงโดยใช้ $ZnNb_2O_6$ เป็นสารตั้งต้นเปรียบเทียบกับวิธีการแบบดั้งเดิม
- [2] การประดิษฐ์และตรวจสอบเซรามิก $Pb(Zn_{1/3}Nb_{2/3})O_3$ ที่มีการเติมสารออกไซด์ลงไป

โดยมีรายละเอียดของแต่ละส่วนดังนี้

1. ศึกษาค้นคว้ารวบรวมข้อมูลจากเอกสารทางวิชาการที่เกี่ยวข้อง
2. ทำการสังเคราะห์สาร $Pb(Zn_{1/3}Nb_{2/3})O_3$ ด้วยวิธีการ mixed oxide แบบดั้งเดิม โดยใช้ PbO , ZnO และ Nb_2O_5 เป็นสารตั้งต้น (ชุดควบคุม)
3. ทำการสังเคราะห์สาร columbite $ZnNb_2O_6$ ด้วยเทคนิค solid-state reaction
4. ทำการสังเคราะห์สาร $Pb(Zn_{1/3}Nb_{2/3})O_3$ ด้วยวิธี mixed oxide แบบดัดแปลงที่ใช้ $ZnNb_2O_6$ (จากข้อที่ 3) เป็นสารตั้งต้น (columbite route)
5. ศึกษาอิทธิพลของปัจจัยในกระบวนการสังเคราะห์สารที่ได้จากข้อ 2-4 ด้วยเทคนิค solid-state reaction ได้แก่ เทคนิคการบดย่อยระยะเวลาในการบดย่อยและเงื่อนไขในการเผา calcination (อุณหภูมิที่ใช้ในการเผา ระยะเวลาในการเผา และอัตราการขึ้น/ลงอุณหภูมิ) ที่มีต่อพฤติกรรมการก่อเกิดเฟสและสัณฐานวิทยา (รูปร่าง ขนาดและการแจกแจงของขนาดอนุภาค)

6. ทำการตรวจวิเคราะห์สารที่เตรียมได้ด้วยการใช้เทคนิคต่างๆร่วมกัน เช่น TGA, DTA, XRD, SEM, TEM, EDX และ laser diffraction เป็นต้น
7. ทำการประดิษฐ์เซรามิก $Pb(Zn_{1/3}Nb_{2/3})O_3$ จากผงที่เตรียมได้ในข้อ 2 และ 4 ด้วยวิธีการเผาซินเตอร์แบบปกติ (pressureless sintering)
8. ทำการคำนวณหาปริมาณเฟสเพอโรพสไกต์และความหนาแน่นสัมพัทธ์ที่ได้จากการเผา sintering ในแต่ละเงื่อนไข นำเสนอกลไกเพื่ออธิบายพฤติกรรมการก่อเกิดเฟส การแน่นตัว และสมบัติทางไฟฟ้าของสารเซรามิก PZN พร้อมทั้งวิเคราะห์เปรียบเทียบผลการทดลองที่ได้
9. ทำการสังเคราะห์สารที่มี $Pb(Zn_{1/3}Nb_{2/3})O_3$ เป็นองค์ประกอบหลักด้วยวิธีการ mixed oxide โดยการเติมสารออกไซด์ชนิดต่างๆ เช่น $Pb(Zr,Ti)O_3$, MnO_2 , Fe_2O_3 และ Al_2O_3 เป็นต้น
10. ทำการประดิษฐ์เซรามิก $Pb(Zn_{1/3}Nb_{2/3})O_3$ จากผงที่เตรียมได้ในข้อ 8.9 ด้วยวิธีการเผาซินเตอร์แบบปกติ
11. ทำการตรวจสอบเซรามิกที่เตรียมได้ทุกสูตรด้วยการใช้เทคนิคต่างๆร่วมกัน เช่น XRD, SEM, TEM, EDX และ dielectric , piezoelectric , ferroelectric measurements เป็นต้น
12. ทำการคำนวณหาปริมาณเฟสเพอโรพสไกต์และความหนาแน่นสัมพัทธ์ที่ได้จากการเผา sintering ในแต่ละเงื่อนไข นำเสนอกลไกเพื่ออธิบายพฤติกรรมการก่อเกิดเฟส การแน่นตัว โครงสร้างจุลภาคและสมบัติทางไฟฟ้าของเซรามิกที่มี $Pb(Zn_{1/3}Nb_{2/3})O_3$ เป็นองค์ประกอบหลัก
13. สรุปผลการศึกษาอิทธิพลของการเติมสารออกไซด์ชนิดต่างๆที่มีต่อพฤติกรรมการก่อเกิดเฟส โครงสร้างจุลภาคและสมบัติทางไฟฟ้าของเซรามิกที่มี $Pb(Zn_{1/3}Nb_{2/3})O_3$ เป็นองค์ประกอบหลัก พร้อมทั้งสรุปความสัมพันธ์ระหว่างปัจจัยในกระบวนการเตรียม การก่อเกิดเฟส โครงสร้างและสมบัติทางไฟฟ้าของวัสดุเหล่านี้
14. นำความรู้ที่ได้จากงานวิจัยตีพิมพ์เผยแพร่ผลการวิจัยลงในวารสารวิชาการระดับนานาชาติ รวมทั้งการนำเสนอในที่ประชุมวิชาการทั้งในและต่างประเทศ

แผนดำเนินงาน	ปีที่ 1											
	1	2	3	4	5	6	7	8	9	10	11	12
1. ศึกษาค้นคว้ารวบรวมข้อมูลที่เกี่ยวข้อง												
2. สั่งซื้อสารเคมีและวัสดุอุปกรณ์ต่างๆ												
3. ทำการสังเคราะห์สาร $ZnNb_2O_6$ และ PZN พร้อมกับการหาเงื่อนไขที่เหมาะสมในการเตรียมผงคุณภาพสูง												
4. ศึกษาอิทธิพลของปัจจัยหลักในกระบวนการสังเคราะห์ที่มีต่อพฤติกรรมการก่อเกิดเฟสและสัณฐานวิทยาของสารแต่ละสูตร												
5. วิเคราะห์ผลและเขียนรายงานความก้าวหน้า												
6. ทำการประดิษฐ์เซรามิก PZN โดยใช้ $ZnNb_2O_6$ เป็นสารตั้งต้นด้วยวิธีการเผาซินเตอร์แบบปกติ												
7. ศึกษาอิทธิพลของปัจจัยหลักในกระบวนการเผา sintering ที่มีต่อพฤติกรรมการก่อเกิดเฟสโครงสร้างจุลภาคและสมบัติทางไฟฟ้าของเซรามิกทุกสูตร												
8. วิเคราะห์ผล เตรียมต้นฉบับเพื่อส่งตีพิมพ์ เผยแพร่และเขียนรายงานประจำปีที่ 1												

แผนดำเนินงาน	ปีที่ 2											
	1	2	3	4	5	6	7	8	9	10	11	12
9. ทำการสังเคราะห์สารที่มี PZN เป็นองค์ประกอบหลัก ด้วยวิธีการ mixed oxide โดยการเติมสารออกไซด์ชนิดต่างๆ	■	■	■	■	■							
10. ศึกษาอิทธิพลของปัจจัยหลักในกระบวนการสังเคราะห์ที่มีต่อพฤติกรรมการก่อเกิดเฟสและสัณฐานวิทยาของสารแต่ละสูตร		■	■	■	■	■						
11. วิเคราะห์ผลและเขียนรายงานความก้าวหน้า			■	■	■	■						
12. ทำการประดิษฐ์เซรามิกที่มี PZN เป็นองค์ประกอบหลักด้วยวิธีการเผาซินเตอร์แบบปกติ							■	■	■			
13. ศึกษาอิทธิพลของปัจจัยหลักในกระบวนการเผา sintering ที่มีต่อพฤติกรรมการก่อเกิดเฟสโครงสร้างจุลภาคและสมบัติทางไฟฟ้าของเซรามิกทุกสูตร								■	■	■	■	
14. วิเคราะห์ผล เตรียมต้นฉบับเพื่อส่งตีพิมพ์ เผยแพร่และเขียนรายงานฉบับสมบูรณ์											■	■

4. สรุปและวิจารณ์ผลการทดลอง และข้อเสนอแนะสำหรับงานวิจัยในอนาคต

โครงการวิจัยนี้ได้พัฒนากระบวนการปรับปรุงสมบัติทางไฟฟ้าของเซรามิกเพอร์โรอิเล็คทริกที่มี เลดซิงค์ในโอเบตเป็นองค์ประกอบหลักด้วยการใช้สารตั้งต้น แบบโคลัมไบต์และการเติมสารออกไซด์ โดยอาศัยวิธีการควบคุมปัจจัยในกระบวนการเตรียมให้มีความเหมาะสม โดยเฉพาะอย่างยิ่ง เงื่อนไขในการเผาแคลไซน์และการเผาซินเทอร์ ซึ่งโครงการนี้ได้แสดงให้เห็นถึงอิทธิพลของปัจจัยในกระบวนการเตรียมที่มีต่อลักษณะเฉพาะของการก่อเกิดเฟส พัฒนาการของโครงสร้างจุลภาคและสมบัติทางไฟฟ้าของสารเซรามิกที่มี PZN เป็นองค์ประกอบหลัก

ข้อเสนอแนะสำหรับงานวิจัยในอนาคต

- (I) การศึกษาวิจัยเพื่อหาวิธีการควบคุมพฤติกรรมในการก่อเกิดเฟสของสารเหล่านี้ที่เหมาะสมเป็นสิ่งที่น่าสนใจมากสำหรับการวิจัยในอนาคต
- (II) การปรับปรุงคุณภาพของชิ้นงานอาจกระทำได้โดยการเลือกใช้เทคโนโลยีที่สูงขึ้นในการเพิ่มความหนาแน่นของผลิตภัณฑ์ อย่างเช่น การเผาชิ้นงานภายใต้บรรยากาศของออกซิเจน
- (III) งานวิจัยในอนาคตที่มุ่งเน้นเรื่องการตรวจสอบสมบัติทางไฟฟ้าของวัสดุเหล่านี้ โดยเฉพาะอย่างยิ่ง สมบัติทางพีโซอิเล็กทริกและสมบัติทางไฟฟ้าเชิงกล น่าจะช่วยให้เสริมสร้างความรู้ความเข้าใจในเรื่องของสารเพอร์โรอิเล็คทริกกลุ่มเพอโรฟสไกต์ให้มีความลึกซึ้งมากยิ่งขึ้น

5. ภาคผนวก

Effect of Al₂O₃ Addition on Dielectric, Piezoelectric and Ferroelectric Properties of 0.2Pb(Zn_{1/3}Nb_{2/3})O₃-0.8Pb(Zr_{1/2}Ti_{1/2})O₃ Ceramics

A. Ngamjarrojana*, S. Ananta and R. Yimnirun

Department of Physics, Faculty of Science, Chiang Mai University, 50200, Thailand.

*Corresponding author. Tel.: +66-53-941921 ext 445; fax: +66-53-943445.

E-mail address: Ngamjarrojana@yahoo.com

Keywords: Dielectric properties, Piezoelectric properties, Ferroelectric properties and Hard doping

Abstract. The structure and electrical properties of Al₂O₃-doped 0.2Pb(Zn_{1/3}Nb_{2/3})O₃-0.8Pb(Zr_{1/2}Ti_{1/2})O₃ ceramic, which is the morphotropic phase boundary composition of the PZN-PZT system, were investigated. The addition of Al₂O₃ content transformed the crystal structure from coexisting with rhombohedral to purely tetragonal structure. Furthermore, addition of Al₂O₃ decreased ϵ_r , d_{33} and k_p , but increased Curie temperature and enhanced the mechanical quality factor. Finally, the P - E and s - E loops demonstrated decreased P_r , E_c and strain level with addition of Al₂O₃.

Introduction

Lead zirconate titanate, Pb(Zr,Ti)O₃ or PZT, is a well known piezoelectric that has been widely employed in a large number of sensing and actuating devices. PZT ceramics have very high Curie temperature (~ 390 °C). Lead zinc niobate, Pb(Zn_{1/3}Nb_{2/3})O₃ or PZN, which exhibits a perovskite structure and a Curie temperature of ~140 °C, is one of the most important relaxor ferroelectric materials with a high dielectric constant and large electrostrictive coefficient. They have excellent dielectric, piezoelectric and elastic properties suitable for wide range of practical applications [1-3]. Though the PZN-PZT based ceramics have excellent electrical properties, poor mechanical properties such as fracture strength and toughness have been reported [4]. In some applications at high power and high stress, mechanical properties of this material become critically important. Recently, it is reported that the mechanical properties of structural ceramics can be improved by an addition of second phase nanoparticles such as SiC and Al₂O₃ [5]. It is therefore of interest to explore the possibility of using Al₂O₃ as both electrical properties modification with possible mechanical properties benefit.

Thus, in this study 0.2Pb(Zn_{1/3}Nb_{2/3})O₃-0.8Pb(Zr_{1/2}Ti_{1/2})O₃ ceramics were prepared and the influences of Al₂O₃ addition on structure, and electrical properties of the ceramics were investigated, which are especially important from the viewpoint of the development of practical piezoelectric materials.

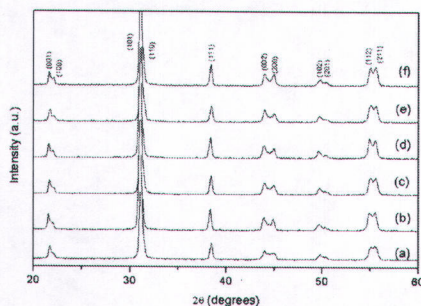
Experimental

The specimens studies were fabricated according to the formula: 0.2Pb(Zn_{1/3}Nb_{2/3})O₃-0.8Pb(Zr_{1/2}Ti_{1/2})O₃+ x wt% Al₂O₃, where $x = 0.1, 0.3, 0.5, 0.7$ and 0.9 . Raw materials of PbO, ZrO₂, TiO₂, ZnO, Nb₂O₅ and Al₂O₃ with >99% purity were used to prepare samples by a conventional mixed oxide process. The starting powders were mixed by zirconia ball media with isopropanol as a medium in a polyethylene jar for 30 min via vibro-milling technique. The mixed slurry was dried and calcined at 900 °C for 2 h. The calcined powders were ball-milled again with additives and consolidated into disks of 12.5 mm diameter using isostatic pressing about 150 MPa. PbO-rich atmosphere sintering of the ceramics was performed in a high-purity alumina crucible at 1200 °C for 2 h. The crystal structure and symmetry of the sintered bodies were examined by X-ray diffraction (XRD) and densities were measured by Archimedes method. Surface morphologies of sintered ceramics were directly imaged, using scanning electron microscopy (SEM; JEOL JSM-840A). Grain size was determined from SEM micrographs by a linear intercept method.

For electrical properties characterizations, silver electrode (Dupont, QS 171) was printed on the lapped surfaces. The electrode was fired at 850 °C for 45 min. The specimens were poled in silicone oil at 150 °C by applying a DC field of 3 kV/mm for 30 min. The dielectric properties of the sintered ceramics were studied as functions of both temperature and frequency with an automated dielectric measurement system. The computer-controlled dielectric measurement system consists of a precision LCR-meter (Hewlett Packard, model 4284A), a temperature chamber, and a computer system. The capacitance and the dielectric loss tangent are determined over the temperature range of 50 and 450 °C with the frequency ranging from 100 Hz to 100 kHz. The Curie temperature (T_c) was determined by the temperature dependence of the dielectric constant at 1 kHz. The piezoelectric constant (d_{33}) was measured using a quasi-static piezoelectric d_{33} meter (Model ZJ-3d, Institute of Acoustics Academic Sinica, China). The planar coupling coefficient (k_p) and the mechanical quality factor (Q_m) were determined by the resonance and anti-resonance technique [6] using an impedance analyzer (Model HP4294A, Hewlett-Packard). Ferroelectric switching measurements were made using a modified Sawyer-Tower circuit with a linear variable differential transducer (LVDT) for strain measurement, DSP lock-in amplifier (SR830, Stanford Research), high voltage power supply (TREK 609C-6, Trek), and computerized control and data acquisition.

Results and Discussion

Figure 1 shows the XRD patterns of Al_2O_3 -doped $0.2\text{Pb}(\text{Zn}_{1/3}\text{Nb}_{2/3})\text{O}_3$ - $0.8\text{Pb}(\text{Zr}_{1/2}\text{Ti}_{1/2})\text{O}_3$ ceramics sintered at 1200 °C for 2 h. In these patterns, the crystal structure of the specimens is modified by the addition of Al_2O_3 , as revealed by the evolution of (200) and (002) peaks. The perovskite structure appears to change from coexisting with rhombohedral to purely tetragonal structure. Slight shift in diffraction angle by doping Al^{3+} ions indicates their substitution (solid solution) into the lattice of PZN-PZT. Al^{3+} ions are expected to substitute B-sites of the perovskite structure because ionic radius of Al^{3+} is closer to that of Zr^{4+} , Ti^{4+} , Zn^{2+} and Nb^{5+} than that of Pb^{2+} [7].



(a) undoped (b) 0.1 wt% (c) 0.3 wt%
(d) 0.5 wt% (e) 0.7 wt% (f) 0.9 wt%

Figure 1. XRD patterns of Al_2O_3 -doped PZN-PZT ceramics sintered at 1200 °C for 2 h.

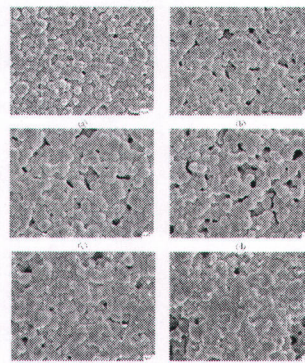


Figure 2. SEM photographs of the surfaces of Al_2O_3 -doped PZN-PZT ceramics

Figure 2 shows SEM photographs of the surfaces of $0.2\text{Pb}(\text{Zn}_{1/3}\text{Nb}_{2/3})\text{O}_3$ - $0.8\text{Pb}(\text{Zr}_{1/2}\text{Ti}_{1/2})\text{O}_3$ ceramics doped with 0.1–0.9 wt% Al_2O_3 . As shown in Fig. 2, the grain sizes of ceramics are slightly increased with increasing amount of Al_2O_3 addition. However, the SEM micrographs in Fig. 2(e-f) show that a higher porosity level is observed when the amount of Al_2O_3 is increased, which indicates that the specimens are not sintered effectively. The above results are obviously consistent with the change in the bulk density with Al_2O_3 content for Al_2O_3 -doped $0.2\text{Pb}(\text{Zn}_{1/3}\text{Nb}_{2/3})\text{O}_3$ - $0.8\text{Pb}(\text{Zr}_{1/2}\text{Ti}_{1/2})\text{O}_3$ ceramics. It can be seen from Fig. 2 that Al ions are mainly

accumulated at the grain boundaries [8]. Atkim *et al.* [9] reported that dopant ions were concentrated at grain boundaries and took excess impurities by diffusion when grain boundaries moved, which in turn reduced grain boundary mobility and size. These inferences are obviously consistent with the changes mentioned above in the microstructures. The micrographs also show that the grain size of the ceramics varies considerably.

The temperature dependences of the dielectric constant (ϵ_r) at 1 kHz for 0.2PZN–0.8PZT + x wt% Al_2O_3 , $x = 0, 0.1, 0.3, 0.5, 0.7$ and 0.9 are plotted in Fig. 3. The observed broadening of the dielectric peaks may be caused from decreasing of density of ceramics and higher porosity. The variation of the Curie temperature (T_c) as a function of composition x is displayed, which shows an increase in T_c with increasing Al_2O_3 content. Thus, the Curie temperature of 0.2PZN–0.8PZT + x wt% Al_2O_3 system can be varied over a range of 340 and 360°C by controlling the content of Al_2O_3 addition in the system.

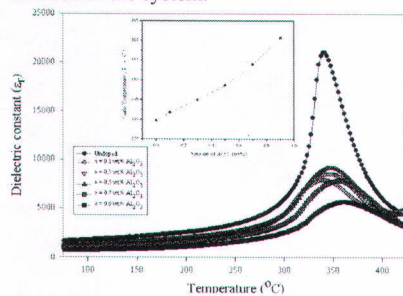


Figure 3. The temperature dependences of the dielectric constant (ϵ_r) at 1 kHz

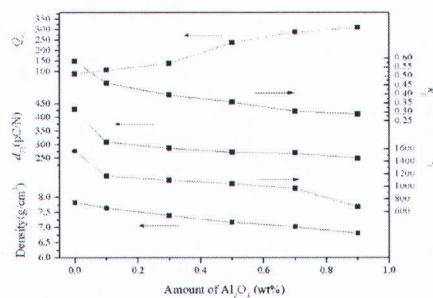


Figure 4. , dielectric constant (ϵ_r), piezoelectric constant (d_{33}), electromechanical coupling factor (k_p) and the mechanical quality factor (Q_m)

Figure 4 shows the changes in density, dielectric constant (ϵ_r), piezoelectric constant (d_{33}), electromechanical coupling factor (k_p) and the mechanical quality factor (Q_m) as a function of the amount of Al_2O_3 addition. With addition of Al_2O_3 , the density, ϵ_r , k_p and d_{33} rapidly decrease. It is well known that the substitutions of acceptor dopant Al ions will lead to the creation of oxygen vacancies, which pin the movement of the ferroelectric domain walls and result in a decrease of ϵ_r , k_p and d_{33} . On the other hand, Q_m rapidly increases with increasing Al_2O_3 content. These observations are in good agreement with previous work by Kulascar *et al.* [10], which reported that in the case of substitution of 3+ ions for B-sites of the perovskite structure, oxygen vacancies produced by charge neutrality beyond solid solution limit lead to decrease in electromechanical coupling factor, dielectric constant and electrical resistivity, and to increase in mechanical quality factor. Hence, these results clearly indicate that increased Al_2O_3 would degrade piezoelectric properties due to exceeding the solution limit of lattices [11].

The polarization-field (P - E) hysteresis loops of 0.2PZN–0.8PZT + x wt% Al_2O_3 ceramics are shown in Fig. 6. The well-developed and fairly symmetric hysteresis loops with the field are observed for all compositions. To further assess ferroelectric characteristics in Al_2O_3 -modified PZN–PZT ceramics, the ferroelectric parameters, i.e. the remnant polarization (P_r) and the coercive field (E_c), have been extracted from the experimental data and given in Table III. It can be seen clearly that P_r , P_s and E_c decrease with an addition of Al_2O_3 into the PZN–PZT composition [12]. Strain of specimens as function of the electric field is shown in Fig. 7. Decreasing in strain and coercive field with increasing Al_2O_3 content is clearly observed. Finally, the decrease in P_r , E_c , and strain level with Al_2O_3 addition suggests the reduction of the polarization and strain that are achieved during an electric field cycle. These quantities depend directly on the extent of domain boundary motion [9].



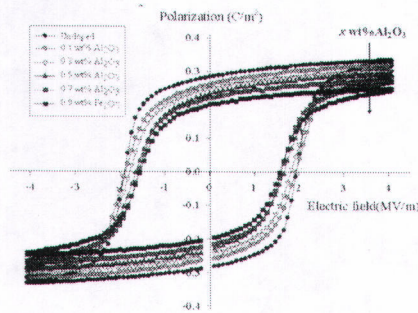


Figure 5. P - E hysteresis loops of 0.2PZN-0.8PZT + x wt% Al_2O_3 ceramics

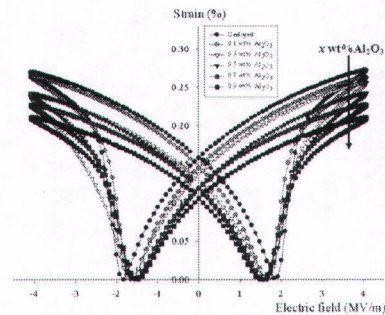


Figure 6. Strain loops of 0.2PZN-0.8PZT + x wt% Al_2O_3 ceramics

Summary

The structure and electrical properties of Al_2O_3 -doped $0.2\text{Pb}(\text{Zn}_{1/3}\text{Nb}_{2/3})\text{O}_3$ - $0.8\text{Pb}(\text{Zr}_{1/2}\text{Ti}_{1/2})\text{O}_3$ ceramic, which is the morphotropic phase boundary composition of the PZN-PZT system, are investigated. The addition of Al_2O_3 transformed the crystal structure from coexisting with rhombohedral to purely tetragonal structure. Furthermore, added Al_2O_3 decreases ϵ_r , d_{33} and k_p , but increases Curie temperature and enhances the mechanical quality factor. The P - E and s - E loops demonstrate decreased P_r , strain level, and E_c when addition of Al_2O_3 in PZN-PZT ceramic systems.

Acknowledgment

This work was jointly supported by the Thailand Research Fund (TRF), Commission on Higher Education (CHE), and the National Nanotechnology Center (NANOTEC), NSTDA, Ministry of Science and Technology, Thailand, through its program of Center of Excellent Network, Faculty of Science, Chiang Mai University. Thanks are also extended to Kenji Uchino, ICAT, Penn State University for helpful discussion and use of facility.

References

- [1] Xu Y.: *Ferroelectric Materials and Their Applications* (Elsevier Science Publishers, Amsterdam, The Netherlands, 1991).
- [2] Uchino K. and Giniewicz J. R.: *Micromechatronics* (Marcel Dekker, New York, 2003).
- [3] Moulson A.J. and Herbert J.M.: *Electroceramics* (2nd ed., Wiley, New York, 2003).
- [4] Tajima K., Hwang H., Sando M. and Niihara K.: *J. Eur. Ceram. Soc.* Vol. 19 (1999), p. 1179.
- [5] Sternitzke M.: *J. Eur. Ceram. Soc.* Vol. 17 (1997), p.1061.
- [6] IEEE Standard on Piezoelectricity: *IEEE Standard 176-1978*. Institute of Electrical and Electronic Engineers, New York, 1978.
- [7] Shannon R. D.: *Acta Crystal. A.* Vol. 32 (1976), p. 751.
- [8] Fang J.X. and Yin Z. W.: *Physics of Dielectric* (Science Press, Beijing, 1989)
- [9] Atkin R. B., and Fularath R. M.: *J. Am. Ceram. Soc.* Vol. 54 (1971), p. 265.
- [10] Kulascar F.: *J. Am. Ceram. Soc.* Vol. 42 (1959), p. 343.
- [11] Kim Y.-M., Kim J.-C., Ur S.-C. and Kim H.-H.: *J. Electroceram.* Vol. 16 (2006), p. 347.
- [12] Iijima T., HeG., Wang Z., Isuboi H., Hiyama K. and Okada M.: *Jpn. J. Appl. Phys.* Vol. 39 (2000), p. 5426.
- [13] Yimnirun R, Ananta, S Ngamjarrojana A, and Wongsanmai S.: *Appl. Phys. A.* Vol. 81 (2005), p. 1227.



Effect of Addition of CuO and Bi₂O₃ on Low Temperature Sintering of Pb(Zr,Ti)O₃ - PbZn_{1/3}Nb_{2/3}O₃ - Pb(Ni_{1/3}Nb_{2/3})O₃ Based Ceramics

Athipong Ngamjarujana

Department of Physics, Faculty of Science, Chiang Mai University, Chiang Mai 50200, Thailand.
Author for correspondence, e-mail: ngamjarujana@yahoo.com

Received: 15 December 2008

Accepted: 2 January 2009.

ABSTRACT

In this study, in order to develop low-temperature-sintering ceramics for a multilayer piezoelectric transformer application, we explored CuO and Bi₂O₃ as sintering aids Pb(Zr,Ti)O₃-Pb(Zn_{1/3}Nb_{2/3})O₃-Pb(Ni_{1/3}Nb_{2/3})O₃ (PZT-PZN-PNN) based ceramics with excellent piezoelectric and dielectric properties such as $d_{33} = 347$ pC/N, $k_t = 0.57$, and $Q_m = 1469$. The addition of CuO decreased the sintering temperature through the formation of a liquid phase. However, the piezoelectric properties of the CuO-added ceramics sintered below 900°C were lower than the desired values. The additional Bi₂O₃ resulted in a significant improvement in the piezoelectric properties. At the sintering temperature of 900°C, the electromechanical coupling factor (k_t), piezoelectric constant (d_{33}), mechanical quality factor (Q_m) of PZT-PZN-PNN composition ceramics with addition of 0.5 wt% CuO and 0.5 wt% Bi₂O₃ showed the optimal value of 0.56, 350 pC/N, and 1042, respectively. These values indicated that the newly developed composition may be suitable for multilayer piezoelectric transformer application.

Keywords: low temperature sintering, piezoelectric transformer and sintering aids.

1. INTRODUCTION

A high electric field and high-vibration level are required for high power piezoelectric devices associated with significant heat generation such as piezoelectric actuators, ultrasonic motors, and piezoelectric transformers. The materials for these applications should have compromised characteristics between hard and soft piezoelectrics, implying high electro-mechanical coupling factor (k) and piezoelectric constant (d) with high mechanical quality factor (Q_m) [1]. However,

the sintering temperature of lead zirconate titanate (PZT)-based high-power compositions is usually too high, approximately 1200°C, to use low metal electrodes such as Ag and Cu. Therefore Ag/Pd alloy is generally used as the electrode to suppress the migration of Ag into the ceramics at high temperature. However, Pd metal is very expensive. Consequently, lowering of the sintering temperature of piezoelectric ceramics is essential for the fabrication of cost-effective

multilayer piezoelectric devices. Furthermore, low temperature sintering can provide advantages such as compatibility with low temperature cofired ceramics (LTCC), the reduction of energy consumption, and the reduced PbO volatilization.

Previously, various techniques were employed to obtain the low temperature sinterable PZT composition. The addition of dopants, which improves solid-state sintering, and the addition of oxides and compounds, which have low melting points for liquid-phase sintering are the most popular methods [2-4]. The other processes such as sintering in an inert atmosphere followed by hot pressing [5], use of fine starting powders [6] are not generally used due to their expensive, complicate and laborious procedure.

Some of the oxides and compounds that have been used for assisting liquid-phase sintering are $\text{BiFeO}_3 + \text{Ba}(\text{Cu}_{1/2}\text{W}_{1/2})\text{O}_3$ [7], Li_2CO_3 , Bi_2O_3 , CdCO_3 [8], LiBiO_2 (melting temperature of 700°C) [9], $4\text{PbOB}_2\text{O}_3$ [10], Bi_2O_3 - Bi_2O_3 - CdO [4], and $\text{PbO} + \text{CuO}$ [11]. Even though these techniques were able to obtain dense ceramics at low sintering temperature, piezoelectric properties were not satisfactory enough to be used in industry. In the initial and middle sintering stages, low temperature sintering aids form a liquid phase and promote densification, but in the final sintering stage, additives enter into a lattice, and eventually affect the dielectric and piezoelectric properties.

Previously, we developed the Sb, Li and Mn substituted $\text{Pb}(\text{Zr}_{0.43}\text{Ti}_{0.52})\text{O}_3$ - $\text{Pb}(\text{Zn}_{1/3}\text{Nb}_{2/3})\text{O}_3$ - $\text{Pb}(\text{Ni}_{1/3}\text{Nb}_{2/3})\text{O}_3$ ceramics with excellent dielectric and piezoelectric properties when sintered at 1200°C [12]. The aim of this study was to lower the sintering temperature of this composition for providing Ag or Cu cofiring compatible high-power piezoelectric ceramics, aiming at layered structure piezoelectric actuators and

transformer applications. We therefore investigated the effect of CuO and Bi_2O_3 addition in the Sb, Li and Mn substituted $\text{Pb}(\text{Zr}_{0.43}\text{Ti}_{0.52})\text{O}_3$ - $\text{Pb}(\text{Zn}_{1/3}\text{Nb}_{2/3})\text{O}_3$ - $\text{Pb}(\text{Ni}_{1/3}\text{Nb}_{2/3})\text{O}_3$ ceramics as a solution for low temperature sinterable high power ceramics.

2. EXPERIMENTAL PROCEDURE

The specimens studied in this research were fabricated according to the formula: $0.8\text{Pb}(\text{Zr}_{0.43}\text{Ti}_{0.52})\text{O}_3 - 0.2\text{Pb} \{0.7\{0.7(\text{Zn}_{0.8}\text{Ni}_{0.2})_{1/3}(\text{Nb}_{0.9}\text{Sb}_{0.1})_{2/3} - 0.3\text{Li}_{1/4}(\text{Nb}_{0.9}\text{Sb}_{0.1})_{3/4}\} - 0.3\text{Mn}_{1/3}(\text{Nb}_{0.9}\text{Sb}_{0.1})_{2/3}\} \text{O}_3 + x \text{ wt}\% \text{CuO} + y \text{ wt}\% \text{Bi}_2\text{O}_3$, called PZT-PZN-PNN based compositions, where $x=0.1\sim 0.5$; $y=0\sim 0.5$, respectively. Raw materials of PbO , ZrO_2 , TiO_2 , ZnO , NiO , Nb_2O_5 , Sb_2O_5 , Li_2CO_3 , MnO_2 , CuO and Bi_2O_3 with $>99\%$ purity were used to prepare samples by a conventional ceramic sintering process. The obtained mixture was ball-milled using zirconia ball media with isopropanol as a medium in a polyethylene jar for 24 h. The mixed slurry was dried and calcined at 750°C for 2 h. The calcined powders were ball-milled again with additives and consolidated into disks of 12.5 mm diameter and rectangular plates using isostatic pressing about 150 MPa. PbO -rich atmosphere sintering of the ceramics was performed in a high-purity alumina crucible at the temperature of $850\text{--}900^\circ\text{C}$ for 2 h. The crystal structure and symmetry of the sintered bodies were examined by X-ray diffraction (XRD) and sintered densities were measured by the Archimedes method. Electrode (Dupont, QS 171) was printed on the lapped surfaces for electrode. The electrode specimens were poled in silicone oil at 150°C by applying a d.c. field of 3kV/mm for 30min. The piezoelectric constant (d_{33}) was measured using a quasi static piezoelectric d_{33} meter (Model ZJ-3d, Institute of Acoustics Academic Sinica, China). The planar coupling coefficient (k_p) and the mechanical quality factor (Q_m) were

determined by the resonance and anti-resonance technique using an impedance analyzer (Model HP4294A, Hewlett-Packard, CA). All ceramics were characterized as described in Figure 1.

3. RESULTS AND DISCUSSION

3.1 Effect of CuO Addition

Initially, the effect of the addition of CuO on PZT-PZN-PNN based ceramics. The sintering temperature of all the specimens was

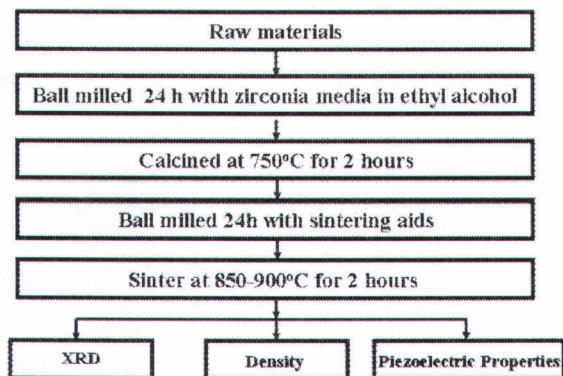


Figure 1. Diagram of experimental procedure on ceramics.

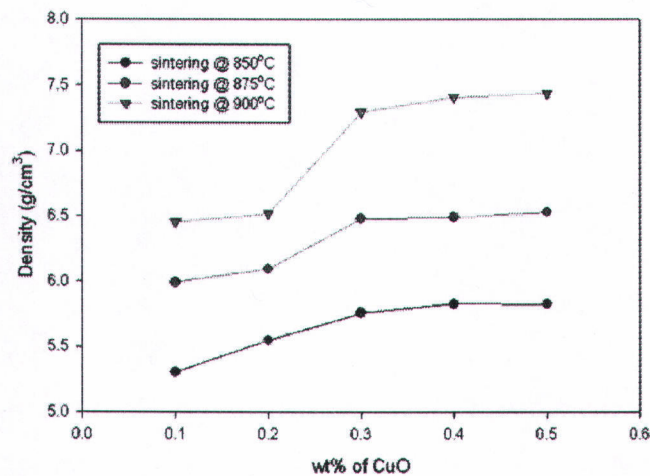


Figure 2. Density in different sintering temperature in PZT-PZN-PNN based compositions + x wt% CuO ceramics.

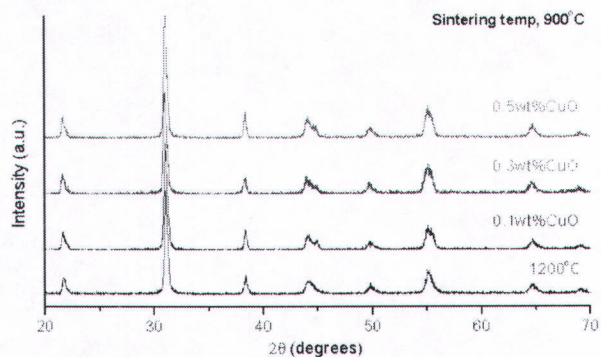


Figure 3. XRD patterns of the samples sintered 900°C for 2h in PZT/PZN-PNN based compositions + x wt% CuO ceramics.

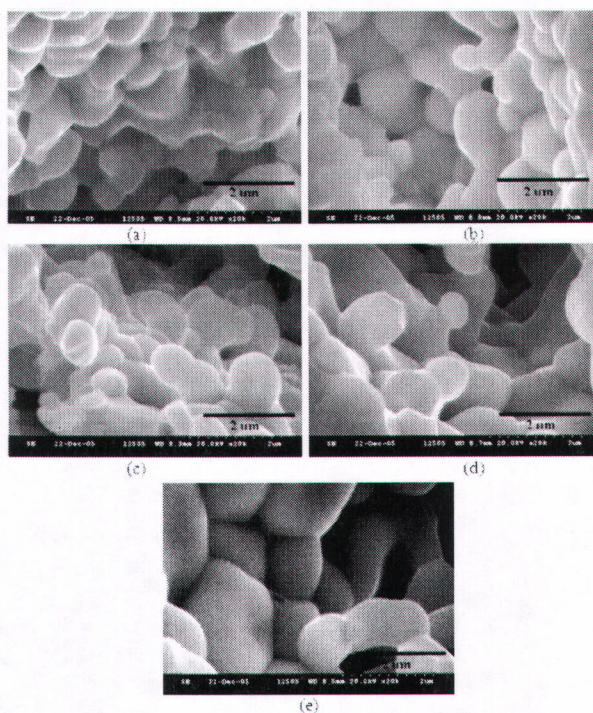


Figure 4. SEM images of the samples sintered at 900°C for 2h in PZT/PZN-PNN based compositions + x wt% CuO ceramics : (a) x=0.1, (b) x=0.2, (c) x=0.3 (d) x=0.4 and (e) x=0.5.

selected with temperatures of 850°C, 875°C, and 900°C, which is cofiring compatible temperature for Ag and low temperature cofired ceramics (LTCC) substrate. Density in different sintering temperature is shown in Figure 2.

Figure 3 shows the XRD patterns of the samples sintered 900°C for 2h in PZT-PZN-PNN based compositions + x wt% CuO ceramics. It can be seen in Figure 3 that all samples exhibit a perovskite structure, and that there is no secondary phase until x=0.2 (any peak for secondary phase was not detected in the range of 0.0-0.2). When x was over 0.3, second phase peak was observed, however, a composition for the second peak was not clearly identified.

Figure 4 shows the SEM images of the PZT-PZN-PNN based compositions + x wt% CuO ceramics sintered at 900°C for 2h. As the CuO addition amount increased, grain growth happened whereas small grains disappeared. This grain growth with CuO addition can be explained with liquid phase sintering. Previously, we showed that the

addition of CuO can reduce the sintering temperature of the $\text{Pb}(\text{Zr,Ti})\text{O}_3\text{-Pb}(\text{Ni,Nb})\text{O}_3$ system by the formation of a liquid phase [13]. Thus this liquid phase formation can also be an explanation for the PZT-PZN-PNN based compositions + x wt% CuO ceramics.

Density, dielectric permittivity ($\epsilon_{33}^T/\epsilon_0$), electromechanical coupling factor (k_p), mechanical quality factor (Q_m) and piezoelectric constant (d_{33}) were plotted as a function of the amount of CuO addition in Figure 5. The density was increased with the increase of CuO contents approximately from 6.4 to 7.8 g/cm³. This improvement of the density might be related to the formation of the liquid phase. Moreover, the variation of piezoelectric and dielectric properties showed similar trend to that of density. Therefore, the improved piezoelectric and dielectric properties, which were observed in the range of x>0.3, might be due to the increased density as well as increased grain size shown in Figure 4. This hardening effect that could be confirmed by the enhancement of Q_m value approximately from 600 to 1200 as shown in Figure 5.

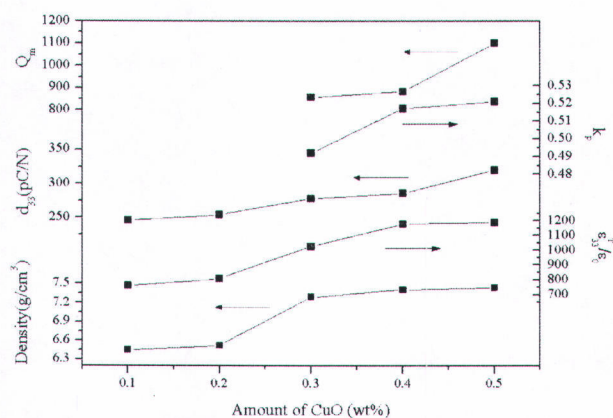


Figure 5. Density, dielectric permittivity ($\epsilon_{33}^T/\epsilon_0$), piezoelectric constant (d_{33}), electromechanical coupling factor (k_p) and mechanical quality factor (Q_m) of the specimens sintered at 900°C for 2h in PZT-PZN-PNN based compositions + x wt% CuO ceramics.

Therefore, Cu ions could be expected to enter B site and act as a hardener.

3.2 Effect of Bi_2O_3 Addition

Bi_2O_3 has low melting temperature (817°C) and it was reported that Bi_2O_3 can form liquid phase with ZnO at approximately 750°C . Therefore, Bi_2O_3 was added to PZT-PZN-PNN based compositions + 0.5 wt% CuO in order to further improve the piezoelectric properties of the specimens sintered at low temperature. Density in different sintering temperature is shown in Figure 6.

Figure 7 shows the XRD patterns of the samples sintered 900°C for 2h in PZT-PZN-PNN based compositions + 0.5 wt% CuO + y wt% Bi_2O_3 ceramics. It can be seen that all the samples exhibit a perovskite structure. The base composition (y=0) had a slight tetragonal symmetry. The tetragonality of the peaks was reduced until y=0.3; but it was

increased when the amount of Bi_2O_3 addition exceeded 0.3 wt%.

Figure 8 shows the SEM images of the PZT-PZN-PNN based compositions + 0.5 wt% CuO + y wt% Bi_2O_3 ceramics sintered at 900°C for 2 h. When the amount of Bi_2O_3 was more than 0.3 wt%, the small grains almost disappeared and average grain size increased. Even though apparent liquid phase formation was not observed in the SEM images, Bi_2O_3 addition might induce small amount of liquid phase and it could be expected to help grain growth due to its low melting point.

Density, dielectric permittivity ($\epsilon_{33}^T/\epsilon_0$), electromechanical coupling factor (k_p), mechanical quality factor (Q_m) and piezoelectric constant (d_{33}) of PZT-PZN-PNN based compositions + 0.5 wt% CuO + y wt% Bi_2O_3 ceramics sintered at 900°C for 2 h are plotted as a function of the amount of Bi_2O_3 addition

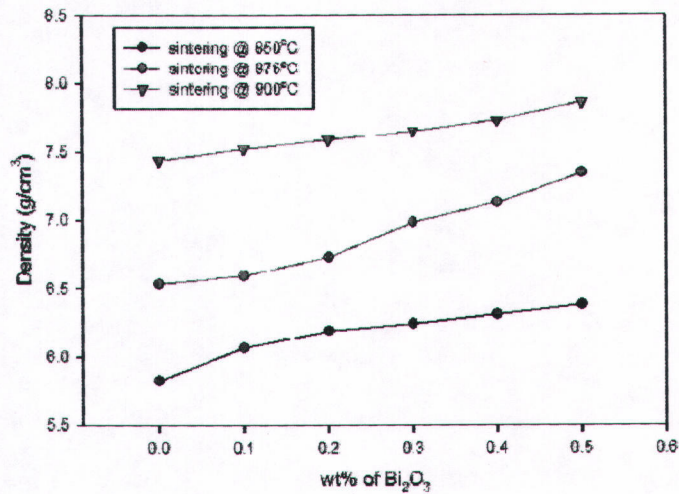


Figure 6. Density in different sintering temperature in PZT-PZN-PNN based compositions + 0.5 wt% CuO + y wt% Bi_2O_3 ceramics.



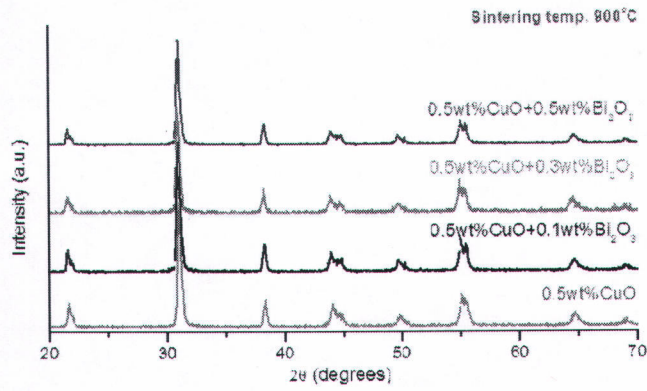


Figure 7. XRD patterns of the samples sintered 900°C for 2h in PZT-PZN-PNN based compositions + 0.5 wt% CuO + y wt% Bi₂O₃ ceramics.

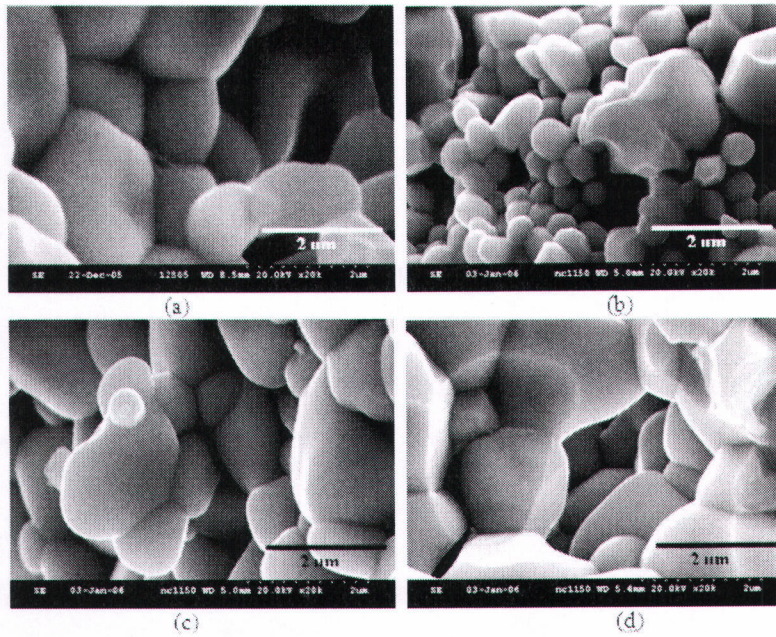


Figure 8. SEM images of the samples sintered at 900°C for 2h in PZT-PZN-PNN based compositions + 0.5 wt% CuO + y wt% Bi₂O₃ ceramics : (a) y=0, (b) y=0.1, (c) y=0.3 and (d) y=0.5.

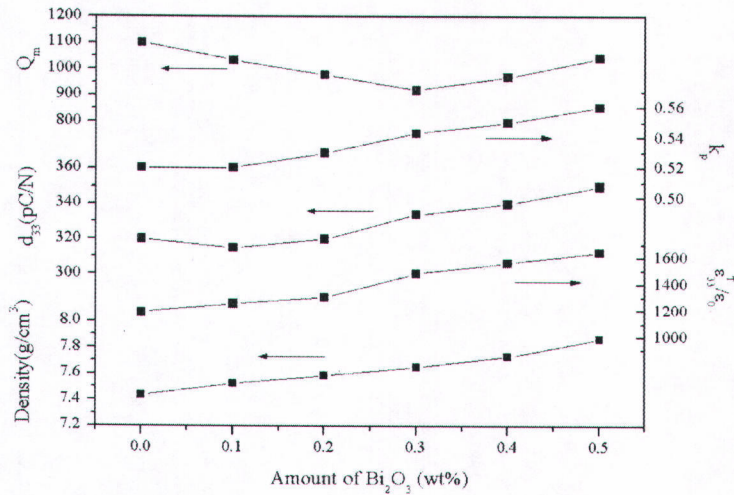


Figure 9. Density, dielectric permittivity ($\epsilon_{33}^T/\epsilon_0$), piezoelectric constant (d_{33}), electromechanical coupling factor (k_p) and mechanical quality factor (Q_m) of the specimens sintered at 900°C for 2h in PZT-PZN-PNN based compositions + 0.5 wt% CuO + y wt% Bi_2O_3 ceramics.

in Figure 9. When Bi_2O_3 was added, density was increased and this increased density improved the dielectric and piezoelectric properties as seen in Figure 8. The density of the specimens was improved when the amount of Bi_2O_3 was added and this increase might be due to the formation of liquid phase. In addition, Q_m was decreased and $\epsilon_{33}^T/\epsilon_0$ and d_{33} were increased with the amount of Bi_2O_3 addition in the range of $0.0 \leq y \leq 0.3$. Therefore, their variations could happen because Bi ions entered A site, since they acted as softener in this range. On the contrary, Q_m exhibits a minimum profile at 0.3 wt% of Bi_2O_3 addition. In addition, $\epsilon_{33}^T/\epsilon_0$, d_{33} and Q_m were increased with the amount of Bi_2O_3 addition above 0.3 wt%. Thus, Bi ions might act as both hardener and softener in this range and their variations might be able to occur because Bi ions entered B site and A site, respectively.

4. CONCLUSIONS

The addition of CuO decreases the sintering temperature through the formation of a liquid phase. However, the piezoelectric properties of the CuO-added ceramics sintered at below 900°C are lower than the desired values. The additional Bi_2O_3 results in a significant improvement in the piezoelectric properties. Furthermore, at the sintering temperature of 900°C, the electromechanical coupling factor (k_p), piezoelectric constant (d_{33}), mechanical quality factor (Q_m) of PZT-PZN based composition ceramics with 0.5 wt% CuO and 0.5 wt% Bi_2O_3 show the optimal value of 0.56, 350 pC/N and 1042, respectively.

5. ACKNOWLEDGEMENTS

This work was supported by the Synchrotron Light Research Institute (Public Organization) SLRI, the Thailand Research Fund (TRF), the Commission on Higher

Education (CHE), and the Faculty of Science, Chiang Mai University. Thank are also extended to Kenji Uchino, ICAT, Penn State for helpful discussion and use of facility during a visit.

REFERENCES

- [1] Uchino K., and Giniewicz J.R., *Micro-mechatronics*, Marcel Dekker, New York, 2003.
- [2] Takahashi S., Sintering Pb(Zr,Ti)O₃ Ceramics at Low Temperature, *Jpn. J. Appl. Phys.*, 1980; **19**: 771-771.
- [3] Lucuta P.G., Constantinescu F., and Barb D., Structural Dependence on Sintering Temperature of Lead Zirconate-Titanate Solid Solutions, *J. Am. Ceram. Soc.*, 1985; **68**: 533-537.
- [4] Zhilun G., Longtu L., Suhua G., and Xiaowen Z., Low-Temperature Sintering of Lead-Based Piezoelectric Ceramics, *J. Am. Ceram. Soc.*, 1989; **72**: 486-491.
- [5] Patel N.D., and Nicholson P.S., Comparison of piezoelectric properties of hot-pressed and sintered PZT, *Am. Ceram. Soc. Bull.*, 1986; **65**: 783-787.
- [6] Yamamoto T., Optimum Preparation Methods for Piezoelectric Ceramics and Their Evaluation, *Am. Ceram. Soc. Bull.*, 1992; **71**: 978-985.
- [7] Kaneko S., Dong D., and Murakami K., Effect of Simultaneous Addition of BiFeO₃ and Ba(Cu_{0.5}W_{0.5})O₃ on Lowering of Sintering Temperature of Pb(Zr,Ti)O₃ Ceramics, *J. Am. Ceram. Soc.*, 1998; **68**: 1013-1018.
- [8] Wang X., Murakami K., and Kaneko S., High-Performance PbZn_{1/3}Sb_{2/3}O₃-PbNi_{1/2}Te_{1/2}O₃-PbZrO₃-PbTiO₃ Ceramics Sintered at a Low Temperature with the Aid of Complex Additives Li₂CO₃-Bi₂O₃-CdCO₃, *Jpn. J. Appl. Phys.*, 2000; **39**: 5556-5559.
- [9] Hayashi T., Inoue T., and Akiyama Y., Low-Temperature Sintering and Properties of (Pb, Ba, Sr)(Zr, Ti, Sb)O₃ Piezoelectric Ceramics Using Sintering Aids, *Jpn. J. Appl. Phys.*, 1999; **38**: 5547-5552.
- [10] Wu L., and Wang C.H., The Dielectric and Piezoelectric Properties of 0.125PMN-0.875PZT Ceramics Doped with 4PbO·B₂O₃, *Jpn. J. Appl. Phys.*, 1993; **32**: 2757-2761.
- [11] Wittmer D.E., and Buchanan R.C., Low Temperature Densification of Lead Zirconate Titanate with Vanadium Pentoxide Additive, *J. Am. Ceram. Soc.*, 1981; **64**: 485-490.
- [12] Park S.-H., Ural S., Ahn C.-W., Nahm S., and Uchino K., Piezoelectric Properties of Sb-, Li-, and Mn-substituted Pb(Zr_xTi_{1-x})O₃-Pb(Zn_{1/3}Nb_{2/3})O₃-Pb(Ni_{1/3}Nb_{2/3})O₃ Ceramics for High-Power Applications, *Jpn. J. Appl. Phys.*, 2006; **45**: 2667-2673.
- [13] Ahn C.-W., Song H.-C., and Nahm S., Priya S., Park S.-H., Uchino K., Lee H.-G., and Lee H.-J., Effect of ZnO and CuO on the Sintering Temperature and Piezoelectric Properties of a Hard Piezoelectric Ceramic, *J. Am. Ceram. Soc.*, 2006; **89**: 921-925.



Effect of MnO_2 Addition on Dielectric, Piezoelectric and Ferroelectric Properties of $0.2Pb(Zn_{1/3}Nb_{2/3})O_3-0.8Pb(Zr_{1/2}Ti_{1/2})O_3$ Ceramics

Athipong Ngamjarurajana, and Supon Ananta*

Department of Physics, Faculty of Science, Chiang Mai University, Chiang Mai 50200, Thailand.

*Author for correspondence; e-mail: suponananta@yahoo.com

Received: 20 December 2008

Accepted: 7 January 2009.

ABSTRACT

Piezoelectric materials are presently being extensively developed for applications such as ultrasonic motors and piezoelectric transformers. In this study the dielectric, piezoelectric, and ferroelectric properties of MnO_2 -doped $0.2Pb(Zn_{1/3}Nb_{2/3})O_3-0.8Pb(Zr_{1/2}Ti_{1/2})O_3$ (hereafter 0.2PZN-0.8PZT), which is the morphotropic phase boundary composition of the PZN-PZT system, were investigated. It was found that crystal structure moved to rhombohedral side when increasing MnO_2 content. With the addition of MnO_2 , Curie temperature T_c , the piezoelectric constant d_{33} , and electromechanical coupling factor k_p were slightly decreased, but the mechanical quality factor Q_m was significantly increased. The P-E and d -E loop demonstrated decreased P_r and strain level but increased E_s with addition of MnO_2 . These results clearly showed the significance of MnO_2 addition on the electrical properties of the PZN-PZT system with "hard" characteristics.

Keywords: dielectric, piezoelectric, ferroelectric, hard doping

1. INTRODUCTION

All commercial piezoelectric devices employ $Pb(Zr,Ti)O_3$ (PZT)-based formulations, close to the morphotropic phase boundary (MPB). The MPB composition is modified by the acceptor and/or donor ions to yield high piezoelectric properties with low losses. The influence of various substitutions on the B-site of $Pb(Zr,Ti)O_3$ perovskite has been widely investigated to optimize the piezoelectric properties [1-6]. Fan and Kim [7] investigated $Pb(Zn_{1/3}Nb_{2/3}\lambda_{1/3})(Zr_{1/2}Ti_{1/2}\lambda_{1/2})O_3$ ceramics with composition close to MPB and clarified that the ceramics had large electro-mechanical coupling factor k_p .

However, the mechanical quality factor Q_m was too low to permit their use as high power piezoelectric devices. It is necessary to improve Q_m as much as possible for suppressing the generation of heat during operation. To develop materials suitable for multilayer piezoelectric transformers and actuators with high d_{33} , high k_p and Q_m , it is necessary to add some dopants in PZN-PZT based ceramics to optimize the piezoelectric properties for device applications [8-11].

Manganese ions have been investigated extensively as effective dopant in PZT-based ceramics because Mn ions can have valence

from Mn^{4+} to Mn^{3+} [1-6, 8-10]. Mn-ions are well known to be effective in very small amounts for improving the reliability of ceramic capacitors. The enhanced properties are expected to be due to the distribution of Mn^{2+} , Mn^{3+} , and Mn^{4+} on B-sites. Mn incorporated on the B sites would act as a lower valent species on a higher valent site. Accordingly, oxygen vacancies would be created for charge compensation, imparting polarization pinning and "hard" characteristics, i.e., an increase in Q_m value [12-14].

In this study, in order to develop PZN-PZT based ceramics for a piezoelectric transducer application, we investigated the influence of MnO_2 addition on structure, and electrical properties of $0.2Pb(Zn_{1/3}Nb_{2/3})O_3$ - $0.8Pb(Zr_{1/2}Ti_{1/2})O_3$ ceramics. The main purpose of this study was to obtain ceramics with higher d_{33} , k_p and Q_m , which are especially important from the viewpoint of the development of practical piezoelectric materials.

2. EXPERIMENTAL PROCEDURE

The specimens studied were fabricated according to the formula: $0.2Pb(Zn_{1/3}Nb_{2/3})O_3$ - $0.8Pb(Zr_{1/2}Ti_{1/2})O_3$ + x wt% MnO_2 , where $x = 0.1, 0.3, 0.5, 0.7$ and 0.9 . Raw materials of PbO , ZrO_2 , TiO_2 , ZnO , Nb_2O_5 and MnO_2 with >99% purity were used to prepare samples by a conventional mixed oxide process. The starting powders were mixed by zirconia ball media with isopropanol as a medium in a polyethylene jar for 30 min via vibro-milling technique. The mixed slurry was dried and calcined at $900^\circ C$ for 2 h. The calcined powders were ball-milled again with additives and consolidated into disks of 12.5 mm diameter using isostatic pressing about 150 MPa. PbO -rich atmosphere sintering of the ceramics was performed in a high purity alumina crucible at $1200^\circ C$ for 2 h. The crystal structure and symmetry of the sintered bodies

were examined by X-ray diffraction (XRD) and densities were measured by Archimedes method. Surface morphologies of sintered ceramics were directly imaged, using scanning electron microscopy (SEM; JEOL JSM-840A). Grain size was determined from SEM micrographs by a linear intercept method.

For electrical properties characterizations, silver electrode (Dupont, QS 171) was printed on the lapped surfaces. The electrode was fired at $850^\circ C$ for 45 min. The specimens were poled in silicone oil at $150^\circ C$ by applying a DC field of 3 kV/mm for 30 min. The dielectric properties of the sintered ceramics were studied as functions of both temperature and frequency with an automated dielectric measurement system. The computer-controlled dielectric measurement system consists of a precision LCR-meter (Hewlett Packard, model 4284A), a temperature chamber, and a computer system. The capacitance and the dielectric loss tangent are determined over the temperature range of 50 and $450^\circ C$ with the frequency ranging from 100 Hz to 100 kHz. The Curie temperature (T_c) was determined by the temperature dependence of the dielectric constant at 1 kHz. The piezoelectric constant (d_{33}) was measured using a quasi-static piezoelectric d_{33} meter (Model ZJ 3d, Institute of Acoustics Academic Sinica, China). The planar coupling coefficient (k_p) and the mechanical quality factor (Q_m) were determined by the resonance and anti-resonance technique [15] using an impedance analyzer (Model HP4294A, Hewlett-Packard). Ferroelectric switching measurements were made using a modified Sawyer-Tower circuit with a linear variable differential transducer (LVDT) for strain measurement, DSP lock-in amplifier (SR830, Stanford Research), high voltage power supply (TREK 609C-6, Trek), and computerized control and data acquisition.

3. RESULTS AND DISCUSSION

Perovskite phase formation, crystal structure and lattice parameter were determined by XRD at room temperature. The XRD patterns of $0.2\text{Pb}(\text{Zn}_{1/3}\text{Nb}_{2/3})\text{O}_3$ - $0.8\text{Pb}(\text{Zr}_{1/2}\text{Ti}_{1/2})\text{O}_3$, with the addition of 0.0-0.9 wt% MnO_2 are shown in Figure 1, showing the perovskite structure for all compositions. The pyrochlore phase is not observed in this system. In the XRD patterns, the crystal structure of the specimens appears clearly to change to rhombohedral side across MPB with increasing amount of MnO_2 around 0.5 wt%. It has been reported [6,8] that manganese coexists mainly in the Mn^{2+} and Mn^{3+} states, which entered into the perovskite structure of BO_6 octahedron to substitute for the B-site ion (e.g, Ti^{4+} and Zr^{4+}).

Figure 2 shows SEM photographs of the surfaces of $0.2\text{Pb}(\text{Zn}_{1/3}\text{Nb}_{2/3})\text{O}_3$ - $0.8\text{Pb}(\text{Zr}_{1/2}\text{Ti}_{1/2})\text{O}_3$ ceramics doped with 0.0-0.9 wt% MnO_2 . As shown in Figs. 2(a-b), the grain sizes of the ceramics are increased with increasing amount of MnO_2 addition. The result is similar to the result of Yu *et al.* [16]. Further increasing MnO_2 content gives rise to an inhomogeneous grain size. However, the SEM micrographs in Figure 2(c-f) show that a higher porosity level is observed when the amount of MnO_2 is increased [17]. The above results are obviously consistent with the

change in the bulk density with MnO_2 content for Mn-doped $0.2\text{Pb}(\text{Zn}_{1/3}\text{Nb}_{2/3})\text{O}_3$ - $0.8\text{Pb}(\text{Zr}_{1/2}\text{Ti}_{1/2})\text{O}_3$ ceramics. It can clearly be seen from Figure 2 that the ceramics have high densities in the MnO_2 addition range of 0.0-0.5 wt%. It is believed that manganese ions are mainly incorporated into the lattice, but if the addition is above 0.5 wt%, manganese ions will accumulate at the grain boundaries [14]. These inferences are obviously consistent with the changes mentioned above in the microstructures. The micrographs also show that the grain size of the ceramics varies considerably, as listed in Table 1.

The temperature and frequency dependences of the dielectric constant (ϵ_r) and dielectric loss tangent ($\tan \delta$) for 0.2PZN - $0.8\text{PZT} + x \text{ wt}\% \text{ MnO}_2$, $x = 0, 0.1, 0.3, 0.5, 0.7$ and 0.9 are shown in Figure 3. The maximum dielectric constant at 1 kHz ($\epsilon_m @ 1 \text{ kHz}$) is listed in Table 2. Dielectric behaviors show strong increase of frequency-dependence on dielectric constant and dielectric loss with increasing amount of MnO_2 . It may be caused from oxygen vacancies and conducting regions near grain boundaries [18] when increasing MnO_2 . The variation of the Curie temperature (T_c) as a function of composition x is plotted in Figure 4. The Curie temperature of 0.2PZN - $0.8\text{PZT} + x \text{ wt}\% \text{ MnO}_2$ system can be varied over a wide range

Table 1. Physical properties of 0.2PZN - $0.8\text{PZT} + x \text{ wt}\% \text{ MnO}_2$ ceramics.

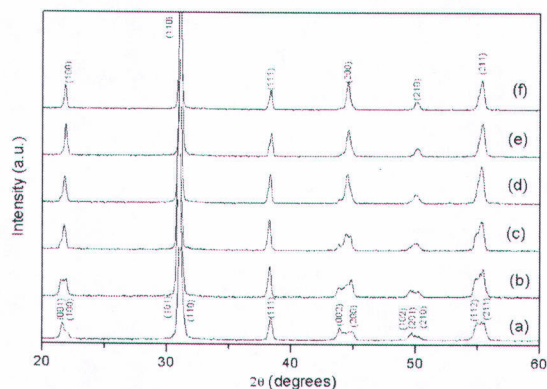
x	Density (g/cm ³)	Grain size range(μm)	Average grain size (μm)
0	7.826	0.5 - 2.0	1.726
0.1	7.849	1.5 - 6.0	4.131
0.3	7.897	1.0 - 3.0	2.991
0.5	8.028	0.5 - 2.0	2.116
0.7	7.718	-	-
0.9	7.653	-	-

Table 2. Dielectric and piezoelectric properties of 0.2PZN–0.8PZT + x wt% MnO₂ ceramics.

x	T_c (°C)	Dielectric properties (at 25 °C, 1 kHz)		Dielectric properties (at T_{Max})		Piezoelectric properties		
		ϵ_r	$\tan\delta$	ϵ_r	$\tan\delta$	d_{33} (pC/N)	k_p	Q_m
0	339.7	1575	0.0249	21047	0.0420	430	0.583	90
0.1	334.2	1155	0.0436	17784	0.1181	365	0.564	356
0.3	326.5	1100	0.0464	19102	0.1241	320	0.551	735
0.5	323.4	1086	0.0440	18220	0.1454	305	0.532	1413
0.7	318.7	1020	0.0368	21178	0.1354	263	0.48	1260
0.9	311	948	0.0438	21389	0.1762	237	0.44	1080

Table 3. Ferroelectric and strain properties of 0.2PZN–0.8PZT + x wt% MnO₂ ceramics .

x	Ferroelectric properties (at 25 °C)			Loop squareness (R_{sq})	Strain %@ 4MV/m
	P_r (C/m ²)	P_s (C/m ²)	E_c (MV/m)		
0	0.287	0.300	1.97	1.483	0.278
0.1	0.224	0.233	2.18	1.488	0.231
0.3	0.208	0.213	2.37	1.712	0.188
0.5	0.147	0.175	1.94	1.024	0.162
0.7	0.089	0.126	1.63	0.811	0.134
0.9	0.077	0.111	1.75	0.811	0.115

**Figure 1.** XRD patterns of the samples sintered at 1200°C for 2h of 0.2PZN–0.8PZT + x wt% MnO₂ ceramics: (a) $x=0$, (b) $x=0.1$, (c) $x=0.3$, (d) $x=0.5$, (e) $x=0.7$ and (f) $x=0.9$.

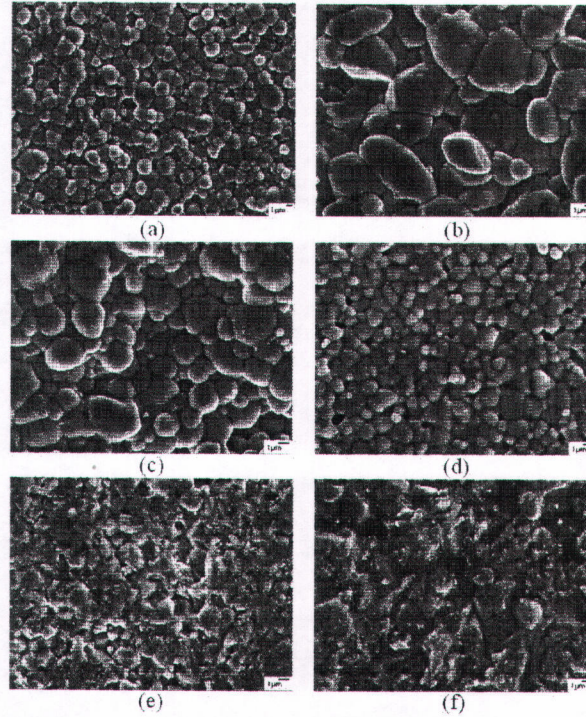


Figure 2. SEM images of the specimens sintered surface of 0.2PZ/N-0.8PZ/1 + x wt% MnO_2 ceramics at 1200°C for 2h; (a) $x=0$, (b) $x=0.1$, (c) $x=0.3$, (d) $x=0.5$, (e) $x=0.7$ and (f) $x=0.9$.

from 310 to 340 °C by controlling the addition of MnO_2 content in the system. The results indicate a rapid decrease in T_c with an increase in MnO_2 content over the range from 0.0 to 0.9 wt%.

Density, dielectric constant (ϵ_r), electro-mechanical coupling factor (k_p), mechanical quality factor and piezoelectric constant (d_{33}) are plotted as a function of amount of MnO_2 addition in Figure 5. When the amount of MnO_2 is lower than 0.5 wt%, density slightly increases. However, ϵ_r , k_p and d_{33} show decreasing trends with increasing MnO_2 content. When the amount of MnO_2 is lower than 0.5 wt%, k_p and d_{33} are rapidly decreased

with increasing MnO_2 content. It is well known that the substitutions of acceptor dopant Mn ions will lead to the creation of oxygen vacancies, which pin the movement of the ferroelectric domain walls and result in a decrease of ϵ_r , k_p and d_{33} [11,19]. The mechanical quality factor (Q_m) increases rapidly with increasing MnO_2 content [4]. The acceptor dopant of MnO_2 improves Q_m significantly. The highest value Q_m (~1413) are obtained in the ceramics with MnO_2 amounts of 0.5 wt%. Further addition of MnO_2 above 0.5 wt% leads to a slightly decrease in the value of Q_m , which may be mainly attributable to non-uniformity of the

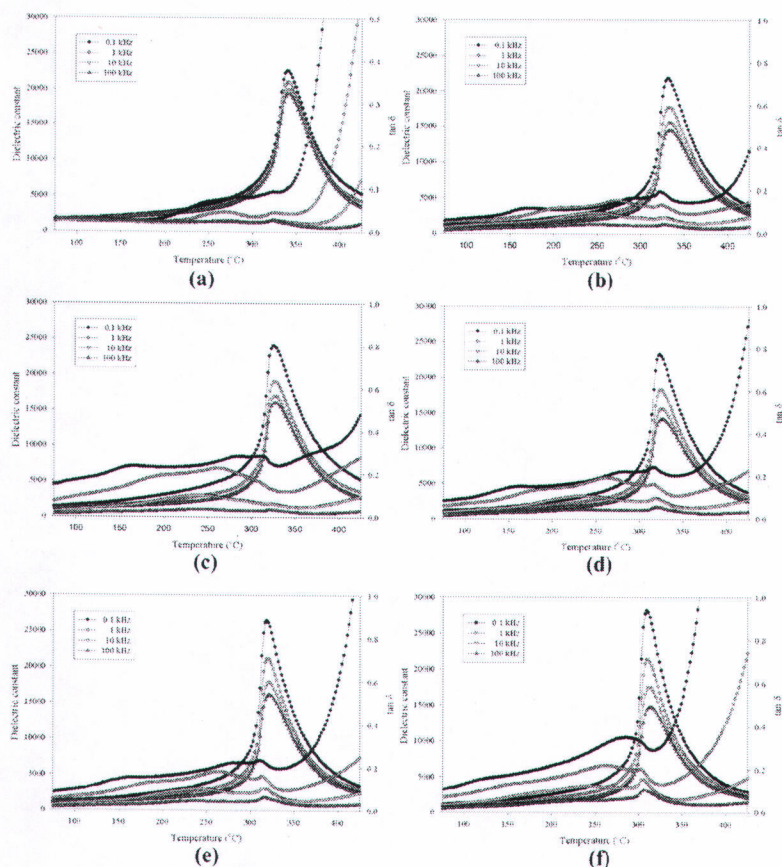


Figure 3. Temperature and frequency dependence of dielectric properties of 0.2PZN-0.8PZT + x wt% MnO_2 ceramics at 1200°C for 2h; (a) $x=0$, (b) $x=0.1$, (c) $x=0.3$, (d) $x=0.5$, (e) $x=0.7$ and (f) $x=0.9$.

microstructure, as shown in Figure 2.

The polarization-field (P - E) hysteresis loops of 0.2PZN-0.8PZT + x wt% MnO_2 ceramics are shown in Figure 6. The well-developed and fairly symmetric hysteresis loops with the field are observed for all compositions. To further assess ferroelectric

characteristics in MnO_2 -modified PZN-PZT ceramics, the ferroelectric parameters, i.e. the remnant polarization (P_r) and the coercive field (E_c), have been extracted from the experimental data and given in Table 3. It can be seen that P_r and P_s decrease with an addition of MnO_2 into the PZN-PZT

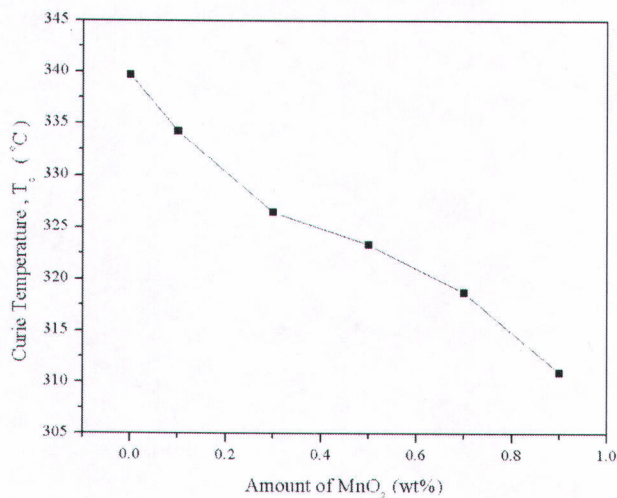


Figure 4. Curie temperature of the specimens sintered at 1200°C for 2h of 0.2PZN–0.8PZ + x wt% MnO₂ ceramics where $x = 0, 0.1, 0.3, 0.5, 0.7$ and 0.9 .

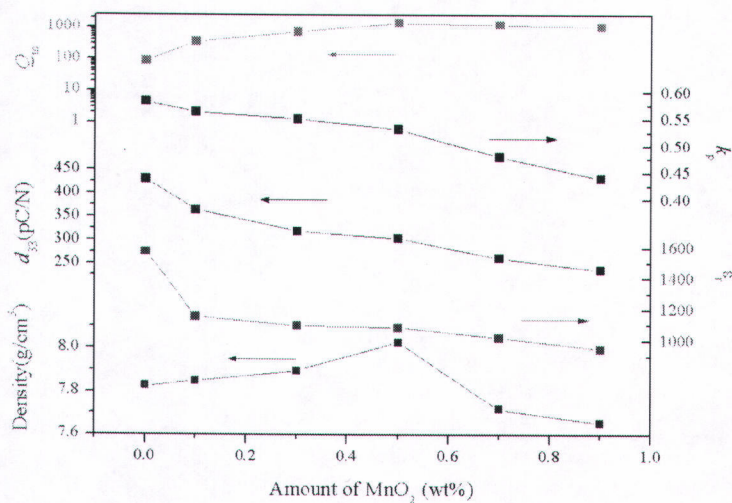


Figure 5. Density, dielectric constant (ϵ_r), piezoelectric constant (d_{33}), electromechanical coupling factor (k_p), and mechanical quality factor (Q_m) of the specimens sintered at 1200°C for 2h of 0.2PZN–0.8PZT + x wt% MnO₂ ceramics where $x = 0, 0.1, 0.3, 0.5, 0.7$ and 0.9 .



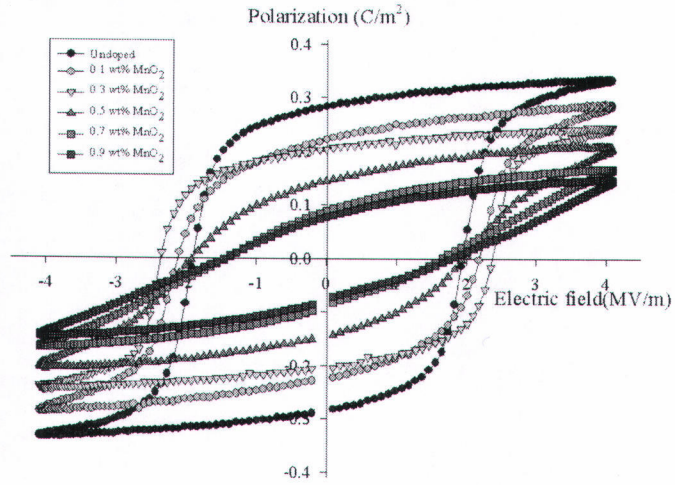


Figure 6. Polarization and electric field (P-E) loops of 0.2PZ/N-0.8PZT + x wt% MnO₂ ceramics.

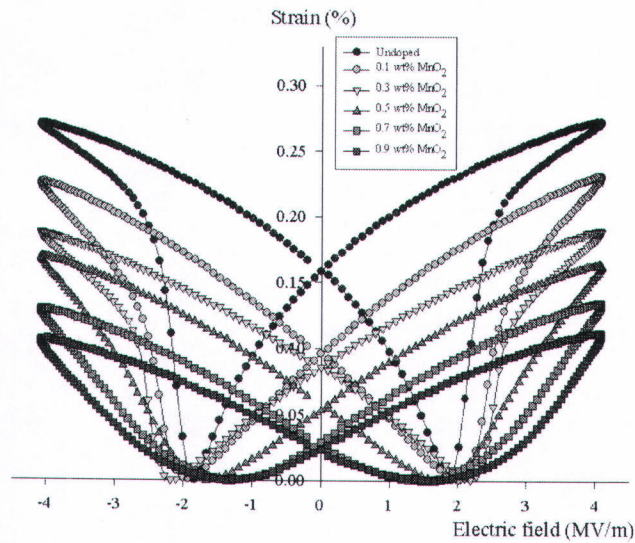


Figure 7. Strain and electric field (s-E) loops of 0.2PZ/N-0.8PZT + x wt% MnO₂ ceramics.

composition, while E_c increases to the maximum at $x = 0.3$ wt%. The ferroelectric characteristics can also be assessed with the hysteresis loop squareness (R_{sq}), which can be calculated from the empirical expression $R_{sq} = (P_r/P_s) + (P_{1.1E_c}/P_s)$, where P_r is the remnant polarization, P_s is the saturated polarization obtained at some finite field strength below the dielectric breakdown and $P_{1.1E_c}$ is the polarization at the field equal to $1.1E_c$ [20]. For the ideal square loop, R_{sq} is equal to 2.00. As listed in Table 3, the R_{sq} parameter increases from 1.483 in $x = 0$ to reach the maximum value of 1.712 in $x = 0.3$. Further addition of MnO_2 above 0.3 wt% leads to a decrease in the R_{sq} parameter, which is mainly attributable to non-uniformity of the microstructure, as shown in Figure 2. The longitudinal strain ($\bar{\epsilon}$) of the specimens as a function of the electric field is shown in Figure 7. The strains are degraded markedly when MnO_2 content is increased, as listed in Table 3. These results (decreased P_r and strain level but increased E_c) clearly indicate the "hard" characteristics with addition of MnO_2 mainly caused by Mn ions substitution in B-site leads to the creation of oxygen vacancies, which pin the movement of the ferroelectric domain walls.

4. CONCLUSIONS

The structure and electrical properties of MnO_2 -doped $0.2Pb(Zn_{1/3}Nb_{2/3})O_3$ - $0.8Pb(Zr_{1/2}Ti_{1/2})O_3$ ceramic, which is the MPB composition of the PZN-PZT system, are investigated. The addition of MnO_2 content transforms the crystal structure to rhombohedral side. Furthermore, MnO_2 addition decreases the Curie temperature, ϵ_r , d_{33} and k_p , but enhances the mechanical quality factor. The P - E and δ - E loops demonstrate decreased P_r and strain level with increased E_c with addition of MnO_2 . These results clearly show the hardening influence of MnO_2

in the PZN-PZT system.

5. ACKNOWLEDGEMENTS

This work was supported by the Synchrotron Light Research Institute (Public Organization) SLRI, the Thailand Research Fund (TRF), the Commission on Higher Education (CHE), and the Faculty of Science, Chiang Mai University.

REFERENCES

- [1] Jin B.M., Kim J., and Kim S.C., Effects of grain size on the electrical properties of $PbZr_{0.52}Ti_{0.48}O_3$ ceramics, *Appl. Phys. A: Mater.*, 1997; **65**: 53-55.
- [2] Yudong H., Mankang Z., and Feng G., Effect of MnO_2 Addition on the Structure and Electrical Properties of $Pb(Zn_{1/3}Nb_{2/3})_{0.20}(Zr_{0.50}Ti_{0.50})_{0.80}O_3$ Ceramics, *J. Am. Ceram. Soc.*, 2004; **87**: 847-850.
- [3] Vasileva T.K., Nadoliisky M.M., and Toshev S.D., Study of PZT ceramics doped with Cr_2O_3 , *Phys. Status Solidi (a)*, 1984; **86**: 109-111.
- [4] Toshio K., Toshimasa S., and Takaaki T., Effects of Manganese Addition on Piezoelectric Properties of $Pb(Zr_{0.5}Ti_{0.5})O_3$, *Jpn. J. Appl. Phys.*, 1992; **31**: 3058-3060.
- [5] Takahashi S., and Takahashi M., Effects of Impurities on the Mechanical Quality Factor of Lead Zirconate Titanate Ceramics, *Jpn. J. Appl. Phys.*, 1972; **11**: 31-35.
- [6] Kim J.S., Yoon K.H., Choi B.H., Park J.O., and Lee J.M., Effects of MnO_2 on the Dielectric and Piezoelectric Properties of $Pb(Zr_{0.52}Ti_{0.48})O_3$ Ceramics, *J. Kor. Ceram. Soc.*, 1990; **27**: 187-194.
- [7] Fan H.Q., and Kim H.E., Effect of Lead Content on the Structure and Electrical Properties of $Pb((Zn_{1/3}Nb_{2/3})_{0.5}(Zr_{0.47}Ti_{0.53})_{0.5})O_3$ Ceramics, *J. Am. Ceram. Soc.*, 2001; **84**: 636-638.

- [8] Xu Y., *Ferroelectric Materials and Their Applications*, Elsevier Science Publishers, Amsterdam, The Netherlands, 1991.
- [9] Uchino K., Giniewicz J.R., *Micromechatronics*, Marcel Dekker, New York, 2003.
- [10] Moulson A.J., and Herbert J.M., *Electroceramics (2nd ed.)*, Wiley, New York, 2003.
- [11] Jaffe B., Cook W.R., and Jaffe H., *Piezoelectric Ceramics*, Academic Press Inc., New York, 1971.
- [12] Yoo J., Hong J., and Suh S., Effect of MnO₂ impurity on the modified PbTiO₃ system ceramics for power supply, *Sens. Actuators*, 1999; **78**: 168-171.
- [13] Priya S., Ph.D. Dissertation, Pennsylvania State University, USA., 2003.
- [14] He L.X., and Li C.E., Effects of addition of MnO on piezoelectric properties of lead zirconate titanate, *J. Mater. Sci.*, 2000; **35**: 2477-2480.
- [15] IEEE Standard on Piezoelectricity, *IEEE Standard 176-1978*, Institute of Electrical and Electronic Engineers, New York, 1978.
- [16] Yu C.-S., Hsieh H.-L., X ray investigation of high oriented (1 - x)PbMg_{1/3}Nb_{2/3}O₃ - (x)PbTiO₃ ceramics, *J. Euro Ceram. Soc.*, 2005; **25**: 2435-2427.
- [17] Hou Y.D., Cui B., Zhu M.K., Wang H., Wang B., Yan H., Tian C.S., Structure and electrical properties of Mn-modified Pb((Zn_{1/3}Nb_{2/3})_{0.20}(Zr_{0.50}Ti_{0.50})_{0.80})O₃ ceramics sintered in a protective powder atmosphere, *Mater. Sci. and Eng. B*, 2004; **111**: 77-81.
- [18] Wersing W., Anomalous dielectric losses in manganese doped lead-titanate-zirconate-ceramics, *Ferroelectrics*, 1978; **22**: 813-815.
- [19] Wut L., Wei C.-C., Wu T.-S., and Teng C.-C., Improved ceramics for piezoelectric devices, *J. Phys. C: Solid State Phys.*, 1983; **16**: 2813-2821.
- [20] Yimnirun R., Ananta S., Ngamjarurojana A., and Wongsanmai S., Uniaxial stress dependence of ferroelectric properties of xPMN-(1-x)PZT ceramic systems, *Appl. Phys. A: Mater.*, 2005; **81**: 1227-1231.

Effect of Vibro- Milling Time on Phase Formation and Particle Size of ZnNbO₆ Nano-powders

Athipong Ngamjarujana^{1*}, Rattikorn Yimnirun² and Supon Ananta¹

¹Department of Physics, Faculty of Science, Chiang Mai University, Chiang Mai 50200 Thailand

²School of Physics, Institute of Science, Suranaree University of Technology, Nakhon Ratchasima 30000 Thailand

Keywords: Zinc niobate; Vibro-milling; solid-state reaction; Microstructure; Dielectric Properties

ABSTRACT

Zinc niobate, ZnNb₂O₆, nanopowders was synthesized by a solid-state reaction via a rapid vibro-milling technique. The effect of milling time on the phase formation and particle size of ZnNb₂O₆ powder was investigated. The formation of the ZnNb₂O₆ phase investigated as a function of calcination conditions by DTA and XRD. The particle size distribution of the calcined powders was determined by laser diffraction technique, while morphology, crystal structure and phase composition were determined via a SEM techniques. In addition, by employing an appropriate choice of milling time, a narrow particle size distribution curve was also observed.

INTRODUCTION

Zinc niobate (ZnNb₂O₆, ZN) is one of the binary niobate compounds which exhibits excellent dielectric properties at microwave frequencies [1-2]. It has very low loss and high dielectric constant and is a promising candidate for application in microwave devices[3-4]. Moreover, the columbite-structured ZnNb₂O₆ is well known as an attractive B-site precursor for the preparation of lead zinc niobate (Pb(Zn_{1/3}Nb_{2/3})O₃ or PZN)-based ferroelectric ceramics used for high performance electromechanical actuators and transducers and piezoelectric ultrasonic motors [5-7]. This is significant because it is very difficult to synthesize those compounds via the conventional solid-state reaction process using oxides as starting materials [8-10]. In the past, ZnNb₂O₆ powders were usually prepared by a solid-state reaction process [11-13]. Recent work by Vittayakorn *et al.* [14] has also shown promise in producing pure phase columbite ZN powders with the conventional mixed-oxide ball milling method technique that used very long heat treatments at ~950-1350 °C for 4h, while Ngamjarujana *et al.*[15] has successfully synthesized ZN powders via a rapid vibro-milling technique, which have been developed as alternatives to the conventional solid-state reaction of mixed oxides. These techniques are aimed at reducing the temperature of preparation of the compound by mixed oxide route.

Therefore, the main purpose of this work is to explore a simple mixed oxide synthetic route for the production of ZnNb₂O₆ (ZN) powders via a rapid vibro-milling technique and to perform milling time, which calcined at 600 °C for 2 h with heating/cooling rates 5 °C/min, on the phase formation and particle size of ZnNb₂O₆ powder was investigated.

EXPERIMENTAL

In this study, starting materials were commercially available zinc oxide, ZnO (Fluka Chemical, 99.9% purity) and niobium oxide, Nb₂O₅ (Aldrich, 99.9% purity). ZnNb₂O₆ powders were synthesized by the solid-state reaction of these raw materials. Ground mixtures of the powders were required with stoichiometric ratio of ZnO and Nb₂O₅ powders. A McCrone vibro-milling technique

was employed in order to combine mixing capacity with a significant time saving. The milling operation was carried out in isopropanol. High purity corundum cylindrical media were used as the milling media. After varied vibro-milling from 0.5- 25 h, and drying at 120 °C, the mixture was calcined at 600 °C for 2 h with heating/cooling rates 5 °C/min[13] in alumina crucible to investigate the phase formation behavior of ZN powders. Calcined powders were subsequently examined by room temperature X-ray diffraction (XRD; Siemens-D500 diffractometer) using Ni-filtered $\text{CuK}\alpha$ radiation to identify the phases formed for the ZN powders. Powder morphologies and particle sizes were directly imaged using scanning electron microscopy (SEM; JEOL JSM-840A). The particle size distributions of the powders were determined by laser diffraction technique (Zetasizer Nano; Malvern Particle Size).

RESULTS AND DISCUSSION

All calcined powders in together different vibro-milling time as shown in Fig. 1. It can be noticed that all conditions is pure phase of ZnNb_2O_6 which are matched in JCPDS file number 30-0873.

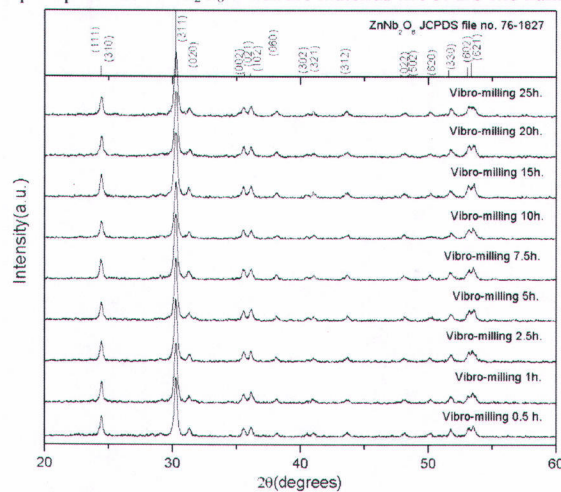


Fig. 1 XRD patterns of the ZN powders calcined at 600 °C for 2 h with heating/cooling rates 5 °C/min with various milling times.

Fig. 2 shows the morphological evolution of all samples as a function of milling times. In general, the particles are agglomerated and basically irregular in shape, with a substantial variation in particle sizes. By increasing the milling time from 0.5 h to 25 h, the particle size of the ZN powder almost similar in size and shape. This is probably due to the effectiveness of vibro-milling and carefully optimized reaction. It is also of interest to point out that larger particle size was obtained for the milling time longer than 10 h. This observation may be attribute to the occurrence of hard agglomeration with strong inter-particle bond within each aggregates resulting from high energy of too long milling time process.

The effect of milling time on particle size distribution was found to be quite significant as shown in Fig 3. After milling times of 0.5–7.5 h, the powders have similar particle size distribution behavior. They exhibit a single peak covering the size ranging from 0.3 – 0.8 μm . By increasing the milling time to 10 h, a uniform particle size distribution with a much lower degree of particle agglomeration was found. However, upon further increasing of milling time up to 25h, a distribution curve with peak broadening between 0.2 – 1 μm was observed. This may be attribute to

the formation of hard and large agglomeration found in the SEM results. In this work, it is seen that the optimum milling time for the production of smallest nanosized and high purity ZN powder was found to be at 10 h. Variations in these data may be attributed mainly to the formation of hard and large agglomerations found in the SEM results.

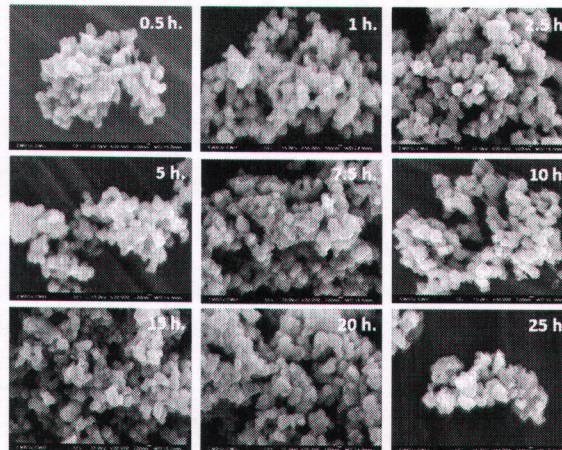


Fig. 2 SEM micrographs of the calcined ZN powders with various milling times.

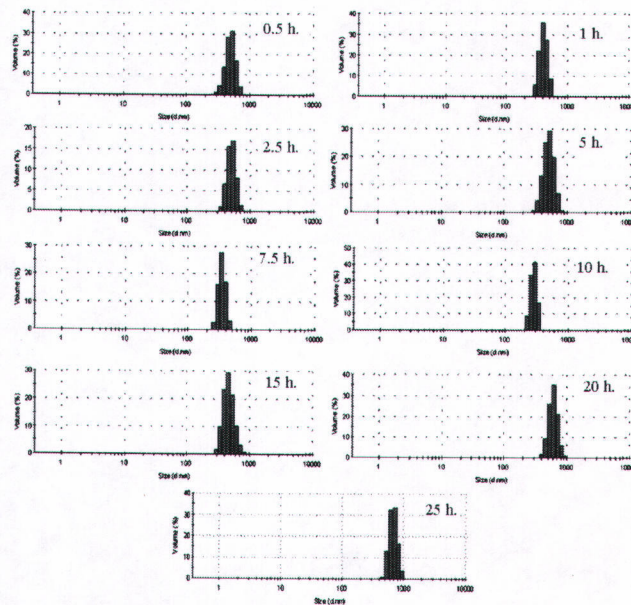


Fig. 3 Particle size distribution curves of the calcined ZN powders with various milling times.

CONCLUSIONS

The effect of milling times on phase formation, particle size and particle size distribution of perovskite zinc niobate synthesized by the solid-state reaction via a rapid vibro-milling technique was investigated. The resulting ZN nano-sized powders consist of a variety of agglomerate particle size, depending on milling times.

ACKNOWLEDGEMENTS

This work was supported by the Thailand Research Fund (TRF), the Commission on Higher Education (CHE) and the Faculty of Science, Chiang Mai University.

REFERENCES

- [1] R. C. Pullar, K. Okeneme and N. M. Alford, *J. Eur. Ceram. Soc.*, 23 (2003) 2479.
- [2] D.W. Kim, K.H. Ko, K.S. Hong, *J. Am. Ceram. Soc.* 84 (6) (2001) 1286.
- [3] A.Z. Simoes, A.H.M. Gonzalez, A.A. Cavalheiro, M.A. Zaghete, B.D. Stojanovic, J.A. Varela, *Ceram. Inter.* 28 (2002) 265.
- [4] L.J. Hu, Y.H. Chang, I.N. Lin, S.J. Yang, *J. Cryst. Growth.* 114 (1991) 191.
- [5] Xu, Y., *Ferroelectric Materials and Their Applications*. Elsevier Science, Amsterdam, The Netherlands, 1991.
- [6] G. Haertling, *J. Am. Ceram. Soc.* 82 (1999) 797.
- [7] A.J. Moulson, J.M. Herbert, *Electroceramics*, 2nd ed., A Wiley-Interscience, New York, 2004
- [8] T.R. Gururaja, A. Safari, A. Halliyal, *Am. Ceram. Soc. Bull.* 65 (1986) 1601.
- [9] M.M.A. Sekar, A. Halliyal, K.C. Patil, *J. Mater. Res.*, 1996, **11**, 1210.
- [10] H.J. Lee, K.S. Hong, S.J. Kim, *Mater. Res. Bull.* 32 (7) (1997) 847.
- [11] Y. Hou, M.K. Zhu, H. Wang, B. Wang, H. Yan, C.S. Tian, *Mater. Lett.* 58 (2004) 1508.
- [12] W. Zhu, A.L. Kholkin, P.Q. Mantas, J.L. Baptista, *J. Am. Ceram. Soc.* 84 (2001) 1740.
- [13] M. Villegas, A.C. Caballero, C. Moure, P. Durán, J.F. Fernández, R.E. Newnham, *J. Am. Ceram. Soc.* 83 (2000) 141.
- [14] N. Vittayakorn, G. Rujijanagul, T. Tunkasiri, X. Tan, D.P. Cann, *J. Mater. Res.*, 2003, **18**, 2882.
- [15] A. Ngamjarrojana, O. Khamman, R. Yimnirun and S. Ananta, *Mater. Lett.* 60 (2006) 2863

e-mail: ngamjarrojana@yahoo.com

Fax: +66-53-943445

GFER #482888, VOL 405, ISS 1

Extended X-Ray Absorption Fine Structure and X-Ray Diffraction Studies of Mn-Doped PZN-PZT Ceramics

Athipong Ngamjarrojana, Laongnuan Srisombat, Rattikorn Yimnirun,
and Supon Ananta

QUERY SHEET

This page lists questions we have about your paper. The numbers displayed at left can be found in the text of the paper for reference. In addition, please review your paper as a whole for correctness.

- Q1.** Au: Please check for empty boxes in text where special characters should be, and provide correct characters.

TABLE OF CONTENTS LISTING

The table of contents for the journal will list your paper exactly as it appears below:

Extended X-Ray Absorption Fine Structure and X-Ray Diffraction Studies of Mn-Doped
PZN-PZT Ceramics

**Athipong Ngamjarrojana, Laongnuan Srisombat, Rattikorn Yimnirun,
and Supon Ananta**

1 **Extended X-Ray Absorption Fine Structure and**
2 **X-Ray Diffraction Studies of Mn-Doped PZN-PZT**
3 **Ceramics**

4 ATHIPONG NGAMJARUROJANA,^{1,4}
5 LAONGNUAN SRISOMBAT,² RATTIKORN YIMNIRUN,³
6 AND SUPON ANANTA^{1,*}

7 ¹Department of Physics and Materials Science, Faculty of Science,
8 Chiang Mai University, Chiang Mai 50200, Thailand

9 ²Department of Chemistry, Faculty of Science, Chiang Mai University,
10 Chiang Mai 50200, Thailand

11 ³School of Physics, Suranaree University of Technology, Nakhon Ratchasima
12 30000, Thailand

13 ⁴ThEP Center, CHE, 328 Si Ayutthaya Road, Bangkok 10400, Thailand

14 *In this work, the selected compositions of a combination between perovskite piezo-*
15 *electric ceramics lead zinc niobate (PZN) and lead zirconate titanate (PZT), close to*
16 *the morphotropic phase boundary (MPB) i.e. the 0.2PZN-0.8PZT, doped with MnO₂*
17 *concentrations of 0.0–0.9 wt% were fabricated by a simple solid-state reaction and a*
18 *pressureless sintering techniques. X-ray diffraction (XRD) spectra from these materi-*
19 *als reveal transformation of the tetragonal into the rhombohedral structure. The local*
20 *structure of Mn was analyzed by mean of synchrotron extended X-ray absorption fine*
21 *structure (EXAFS) measurements at the Mn K-edge. The correlation between the struc-*
22 *tural changes and the Mn content was analyzed and compared. The EXAFS analysis*
23 *indicates that Mn ions should occupy the B-sites in PZN-PZT structure and plays a*
24 *critical role for the hard ferroelectric behavior of the materials.*

25 **Keywords** Piezoceramics; perovskite; EXAFS; X-ray diffraction

26 **1. Introduction**

27 Lead-based complex perovskite piezoceramics with general formula $Pb(B''B''')O_3$ such
28 as PZN, PZT and their solid-solutions close to the MPB are very attractive for sensor,
29 transducer and actuator applications [1–3]. This is because of their low firing temperature
30 and excellent piezoelectric properties. It has been widely proposed that these important
31 properties strongly depend on the rotations and distortions of the BO_6 octahedra [1, 2].
32 Manganese oxide is one of the key effective dopants for lead-based perovskite piezocer-
33 amics to exhibit hard ferroelectric behavior [4–6]. Because of different valence of Mn and
34 B-site ions, an enhancement in the Mn/B-site ions ratio may increase the vacancy concen-
35 tration, forming acceptor-type defects and/or etc. In our previous work [7], the structure

Q1

Received August 23, 2009; in final form October 9, 2009.

*Corresponding author. E-mail: suponananta@yahoo.com

[1]/1

2/[2]

A. Ngamjarujana et al.

36 and electrical properties of MnO₂-doped 0.2PZN-0.8PZT compositions were investigated.
37 It was found that with the addition of MnO₂, Curie temperature, the piezoelectric constant
38 and electromechanical coupling factor were slightly decreased, but the mechanical quality
39 factor was significantly enhanced. However, so far, the nature of the hard ferroelectric re-
40 sponse and the site preference of Mn in these complex perovskite materials are still unclear
41 [4–7]. Additionally, these previous investigation on Mn-doped PZT-based ceramics has
42 also assumed that Mn ions sit in B-site [4–7]. Interestingly, so far, there has been no direct
43 experimental determination of Mn-site in these materials. Thus, in this work, a combina-
44 tion of X-ray diffraction (XRD) and synchrotron extended X-ray absorption fine structure
45 (EXAFS) experiments [8, 9], which is proven to be a powerful technique for resolving the
46 local structure surrounding a particular (absorbing) atom, was performed on the Mn-doped
47 PZN-PZT system in order to determine the local structure around Mn ions.
48

49 2. Experimental

50 The selected samples studied were fabricated according to the formula 0.2Pb(Zn_{1/3}Nb_{2/3})
51 O₃.0.8Pb(Zr_{1/2}Ti_{1/2})O₃ + x wt% MnO₂, where x = 0.0 to 0.9 by a simple mixed-oxide
52 method as detail described elsewhere [7]. Starting materials of PbO, ZnO, Nb₂O₅, ZrO₂,
53 TiO₂, and MnO₂ with >99% purity were vibro-milled with zirconia media in isopropanol
54 for 30 min. After drying, the powders were calcined at 900°C for 2 h. The calcined PZN-
55 PZT powders were vibro-milled with MnO₂ additive and PVA binder for 30 min, pressed
56 into pellets and fired at 500°C for 1 h to eliminate the PVA, followed by sintering with PbO-
57 rich atmosphere inside sealed alumina crucible at 1200°C for 2 h [7]. Phase identification
58 of the samples was performed by XRD and densities were measured by Archimedes
59 method. The synchrotron EXAFS measurement was performed in the transmission mode
60 at the X-ray absorption spectroscopy beamline (BL-8) of the Siam photon source (electron
61 energy of 1.2 GeV), Synchrotron Light Research Institute (Public Organization), Thailand
62 (Fig. 1). The spectra were collected at ambient temperature with a Ge(111) double crystal

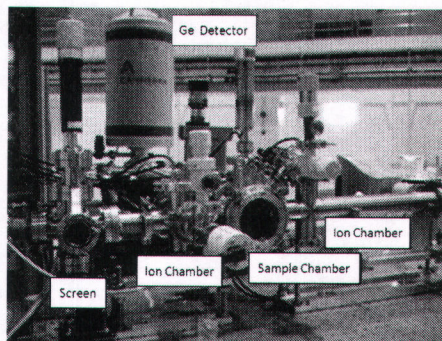


Figure 1. EXAF experimental set-up at BL8, SPS.



63 monochromator and recorded after performing an energy calibration. To increase the count
 64 rate, the ionization chamber was filled with Ar gas. The storage ring was running at an
 65 energy of 1.2 GeV with electron currents between 80 mA and 30 mA.

66 3. Results and Discussion

67 The XRD patterns of $0.2\text{Pb}(\text{Zn}_{1/3}\text{Nb}_{2/3})\text{O}_3-0.8\text{Pb}(\text{Zr}_{0.52}\text{Ti}_{0.48})\text{O}_3$ ceramics at different Mn
 68 concentrations are shown in Fig. 2. In general, the strongest reflections apparent in the
 69 majority of these XRD patterns indicate the formation of the pure perovskite phase for
 70 all compositions. It should be noted that no evidence of the pyrochlore-type compounds
 71 [10, 11] was found in this study, nor was there any indication of the unreacted precursors
 72 [12] being present. This is possibly due to uses of different processing methods. In those
 73 either works, a conventional ball-milling was employed, while the rapid vibro-milling used
 74 in this present study results in finer powders with apparently more reactivity, hence the
 75 pure perovskite phase is formed more easily. Furthermore, the effective suppression of
 76 PbO volatilization commonly found for lead-based perovskite ceramics during high firing
 77 temperature [1, 2] was also achieved with the designed sample arrangement for the sintering
 78 scheme [7] The undoped PZN-PZT ceramics were characterized as tetragonal phase which
 79 is indicated by the splitting of $(002)_T$ and $(200)_T$ peaks in the 2θ range from 43 to 45° , similar
 80 to the reported by Hou *et al.* [13] and Yang *et al.* [14]. It is noticed that a small amount
 81 of rhombohedral phase is also present with increasing Mn substitution with a complete
 82 transformation to rhombohedral phase (revealed by the single $(202)_R$ peak) when x reaches
 83 0.5 wt%). This is similar to the circumstance of PZN (rhombohedral phase) addition on
 84 PZT system earlier reported by Lee *et al.* [11]. In addition, the effect of Mn on the shift
 85 of MPB toward the rhombohedral phase region in the similar system of Mn-doped PZT
 86 ceramics was also observed by Kim and Yoon [6]. It is believed that manganese ions are
 87 mainly incorporated into the lattice, but if the addition is above 0.5 wt%, manganese ions
 88 will accumulate at the grain boundaries [5]. It has been reported that manganese coexists
 89 mainly in the Mn^{2+} and Mn^{3+} states, which entered into the perovskite structure of BO_6
 90 octahedron to substitute for the B-site ion (e.g. Ti^{4+} and Zr^{4+}).

91 The MPB composition range has believed to be quite narrow, but in practice the MPB
 92 has a wide range of compositions over which the tetragonal and rhombohedral phases
 93 coexist in ceramics. Since all properties take extreme values near MPB, the width of the
 94 MPB has been investigated by many workers and found to be related to the heterogeneous
 95 distribution of Zr^{4+} and Ti^{4+} cations on the B-site of perovskite lattice [5, 6]. By means
 96 of XRD, the co-existence of the two phases over a range of compositions around the MPB
 97 was demonstrated in this work. The smaller ionic radius of Mn^{4+} ion (0.053 nm) compared
 98 with that of the B-site ions (either Zn^{2+} (0.083 nm), Nb^{5+} (0.069 nm), Zr^{4+} (0.082 nm) or
 99 Ti^{4+} (0.064 nm) [1, 15] leads to the reductions in the lattice constants (and tetragonality)
 100 in Mn-doped PZN-PZT ceramics. However, the information on site preference of Mn in
 101 PZN-PZT perovskite structure cannot be retrieved directly from the XRD analysis alone.
 102 The EXAFS analysis was then employed to further study the local structure of Mn in the
 103 PZN-PZT-based lattice.

104 Figure 3 show the Mn K edge and Fourier transforms for the EXAFS spectra with
 105 possible bonding information identified and local structure of Mn-doped $0.2\text{PZN}-0.8\text{PZT}$
 106 ceramics. The Fourier transform is a complex function of distance R , the amplitude of
 107 which is denoted by the real function $\rho(R)$. The position of peaks in $\rho(R)$ is related to
 108 bond distances between the Mn ion and neighboring ions while the height of each peak
 109 is proportional to the number of neighbors. The bond lengths and coordination numbers

4/14

A. Ngamjarrojana et al.

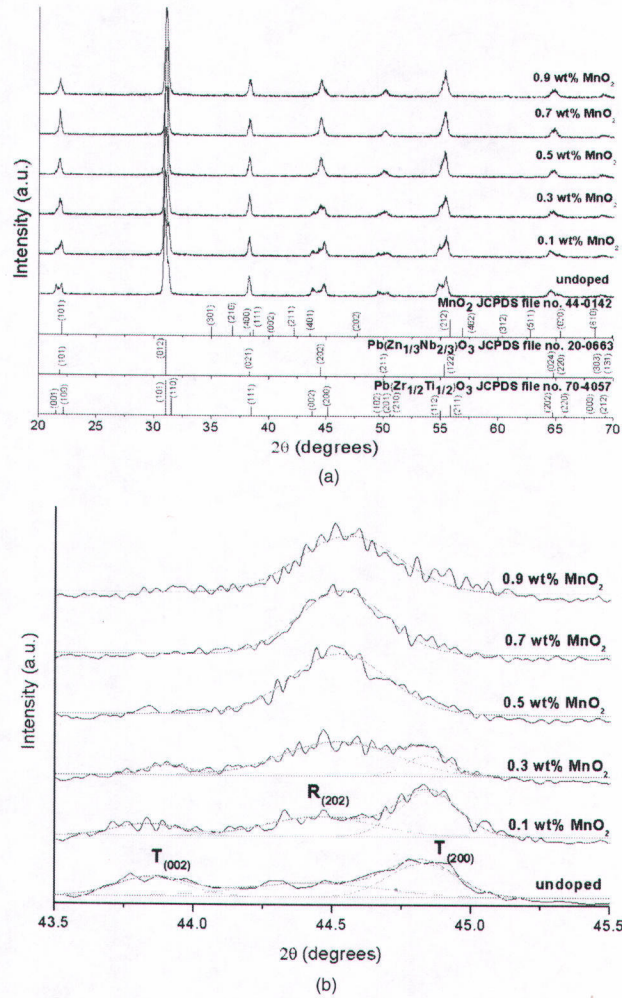
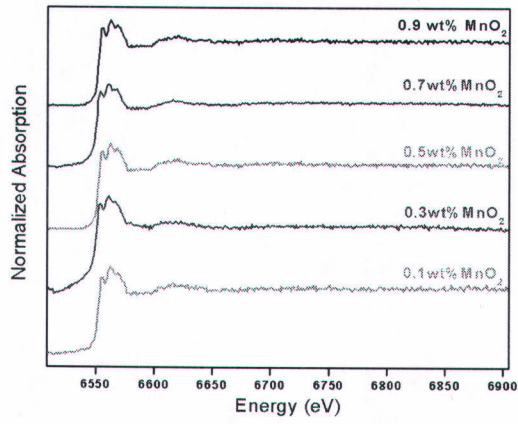


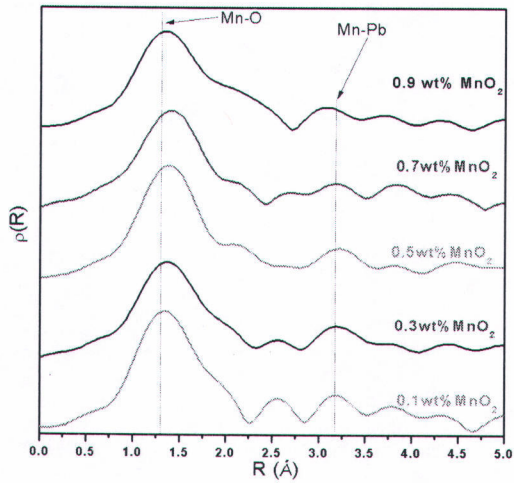
Figure 2. (a) XRD patterns of $0.2\text{Pb}(\text{Zn}_{1/3}\text{Nb}_{2/3})\text{O}_3$, $0.8\text{Pb}(\text{Zr}_{1/2}\text{Ti}_{1/2})\text{O}_3 + x \text{ wt}\% \text{MnO}_2$, where $x = 0.0$ to 0.9 and (b) enlarged XRD patterns in the $2\theta = 43\text{--}46^\circ$. (See Color Plate XXX)

Mn-Doped PAN-PZT Ceramics

15/5



(a)



(b)

Figure 3. (a) Mn K edge spectra of MnO₂ doped 0.2PZN-0.8PZT ceramics, (b) Fourier transforms of the EXAFS spectra for MnO₂ doped 0.2PZN-0.8PZT ceramics (peaks are designed with possible bonding) and (c) Possible local structure for Mn-doped 0.2PZN-0.8PZT ceramics. (See Color Plate XXX)

6/[6]

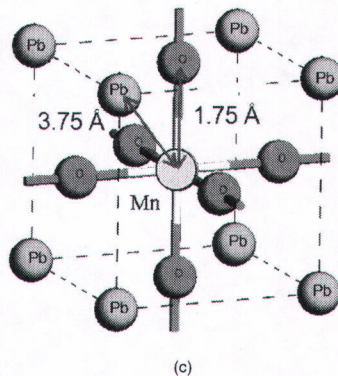
A. Ngamjarrojana *et al.*

Figure 3. (Continued)

110 cannot, however, be read directly from $\rho(R)$. In order to determine the bond lengths and
 111 coordination numbers, the k -dependent amplitude and phase corrections must be made
 112 to the EXAFS signal. For example, prior to the phase correction, the peaks in $\rho(R)$ are
 113 basically smaller than the corresponding bond lengths by ~ 0.5 Å [9]. Interestingly, the
 114 location of Mn within PZN-PZT unit cell can be resolved without making phase and
 115 amplitude corrections. As shown in Fig. 3, by simply comparing the raw Fourier transform
 116 for different Mn contents (0.1–0.9 wt%), there is no observable change in peak positions,
 117 particularly for the first main peak. The coincidence of the main peaks is evidence that no
 118 change in the location of the majority of Mn ions occurs with increasing Mn concentration.
 119 Furthermore, the location of Mn appears to be unaffected by the presence of 0.9 wt%
 120 MnO_2 . It should be noted that a similar Fourier transform of EXAFS spectra for Mn doped
 121 PZN-PZT in this study, Mn doped PZT reported by Cherdhirunkorn *et al.* [9] and PZN,
 122 PZT perovskite established by Chen [16] is observed. The results indicate the site of Mn
 123 atom at B(Zn,Nb,Zr,Ti)-site in the PZN-PZT unit cell. Since the peak position indicates the
 124 bond distance between Mn and its neighbors or the location of Mn within the PZN-PZT unit
 125 cell, the unit cell of Mn-doped PZN-PZT can be extracted from the peak positions in the
 126 Fourier transform of EXAFS spectra shown in Fig. 3. According to the simulation EXAFS
 127 for Mn-doped PZT established by Cherdhirunkorn *et al.* [9], similar information can be
 128 extracted from the Fourier transforms of the EXAFS spectra from Mn-doped PZN-PZT
 129 observed in this work. It is very interesting to observe similar EXAFS signatures between
 130 the Mn-B-site curve where the first main peak occurring at ~ 1.25 Å (due to the six nearest
 131 oxygen atoms), while the second peak at ~ 3.2 Å is attributed to the nearest Pb atoms.
 132 Furthermore by comparing the results shown in Fig. 3 and Ref. [16], it is evident that the
 133 peaks are well consistent with a simulation of EXAFS that assumes Mn occupies the B-site
 134 but the minority A-site occupation cannot be ruled out.

135 **4. Conclusions**

136 A combination of X-ray diffraction and synchrotron extended X-ray absorption fine structure
 137 experiments is performed on Mn-doped $0.2\text{Pb}(\text{Zn}_{1/3}\text{Nb}_{2/3})\text{O}_3\text{-}0.8\text{Pb}(\text{Zr}_{1/2}\text{Ti}_{1/2})\text{O}_3$. The
 138 transformation of the tetragonal into the rhombohedral structure with increasing Mn content
 139 was revealed by XRD technique. The EXAFS analysis indicates that Mn ions should
 140 occupy the B(Zn, Nb, Zr, Ti)-sites in PZN-PZT structure and plays a critical role for the
 141 hard ferroelectric behavior of the materials.

142 **Acknowledgment**

143 This work was supported by the Synchrotron Light Research Institute (Public Organization),
 144 Thailand (GRANT 1-2551/PS02) and the Faculty of Science, Chiang Mai University.

145 **References**

- 146 1. A. J. Moulson and J. M. Herbert, *Electroceramics*. New York: Wiley-Interscience (2003).
 147 2. Y. Xu, *Ferroelectric Materials and Their Applications*. Los Angeles: North Holland (1991).
 148 3. K. Uchino, *Ferroelectric Devices*. New York: Marcel Dekker (2000).
 149 4. Y. Hou, M. Zhu, F. Gao, H. Wang, B. Wang, H. Yan, and C. Tian, Effect of MnO_2 addition on
 150 the structure and electrical properties of $\text{Pb}(\text{Zn}_{1/3}\text{Nb}_{2/3})_{0.20}(\text{Zr}_{0.50}\text{Ti}_{0.50})_{0.80}\text{O}_3$ ceramics. *J. Am.*
 151 *Ceram Soc.* **87**, 847–850 (2004).
 152 5. L. X. He and C. E. Li, Effects of addition of MnO on piezoelectric properties of lead zirconate
 153 titanate. *J. Mater. Sci.* **35**, 2477–2480 (2000).
 154 6. J. S. Kim and K. H. Yoon, Physical and electrical properties of MnO_2 -doped $\text{Pb}(\text{Zr}_x\text{Ti}_{1-x})\text{O}_3$
 155 Ceramics. *J. Mater. Sci.* **29**, 809–815 (1994).
 156 7. A. Ngamjarrojajana and S. Ananta, Effect of MnO_2 addition on dielectric, piezoelectric and
 157 ferroelectric properties of $0.2\text{Pb}(\text{Zn}_{1/3}\text{Nb}_{2/3})\text{O}_3\text{-}0.8\text{Pb}(\text{Zr}_{1/2}\text{Ti}_{1/2})\text{O}_3$ ceramics. *Chiang Mai J.*
 158 *Sci.* **36**, 59–68 (2009).
 159 8. E. R. Kipkoech, F. Azough, R. Freer, and J. F. Mosselmans, Extended x-ray absorption fine
 160 structure analysis of $(\text{Cd},\text{Nd})(\text{Ti},\text{Al})\text{O}_3$ perovskite ceramics used in cellular base stations. *Acta*
 161 *Mater.* **54**, 2305–2309 (2006).
 162 9. B. Cherdhirunkorn, M. F. Smith, S. Limpjumnong, and D. A. Hall, EXAFS study on the site
 163 preference of Mn in perovskite structure of PZT ceramics. *Ceram Inter.* **34**, 727–729 (2008).
 164 10. S. Zhao, H. Wu, and Q. Sun, Study on PSN-PZN-PZT quaternary piezoelectric ceramics near
 165 the morphotropic phase boundary. *Mater. Sci. Eng. B* **123**, 203–210 (2005).
 166 11. S. H. Lee, C. B. Yoon, S. M. Lee, and H. E. Kim, Reaction sintering of lead zinc niobate-lead
 167 zirconate titanate ceramics. *J. Eur. Ceram Soc.* **26**, 111–115 (2006).
 168 12. D. H. Suh, N. K. Kim, and J. H. Kim, Crystallographic and dielectric studies on $\text{Pb}(\text{Zn}_{1/3}\text{Ta}_{2/3})\text{O}_3\text{-}$
 169 substituted $\text{Pb}((\text{Zn}_{1/3}\text{Nb}_{2/3}),\text{Ti})\text{O}_3$ system. *Mater. Lett.* **50**, 6–11 (2001).
 170 13. Y. Hou, M. Zhu, H. Wang, B. Wang, H. Yan, and C. Tian, Effects of CuO addition on the structure
 171 and electrical properties of low temperature sintered $\text{Pb}(\text{Zn}_{1/3}\text{Nb}_{2/3})_{0.20}(\text{Zr}_{0.50}\text{Ti}_{0.50})_{0.80}\text{O}_3$
 172 ceramics. *Mater. Sci. Eng. B* **110**, 27–31 (2004).
 173 14. Z. Yang, H. Li, X. Zong, and Y. Chang, Structure and electrical properties of PZT-PMS-PZN
 174 piezoelectric ceramics. *J. Eur. Ceram Soc.* **26**, 3197–3202 (2006).
 175 15. R. D. Shannon and C. T. Prewitt, Effective ionic radii in oxides and fluorites. *Acta Crystallogr.*
 176 *B* **25**, 925–946 (1969).
 177 16. I. W. Chen, Structural origin of relaxor ferroelectrics-revisited. *J. Phys. Chem. Solid.* **61**, 197–208
 178 (2000).



